Draft version April 25, 2018
Typeset using LaTeX **twocolumn** style in AASTeX61

THE SOLAR NEIGHBORHOOD XLV. THE STELLAR MULTIPLICITY RATE OF M DWARFS WITHIN 25 PC

Jennifer G. Winters,[1,*] Todd J. Henry,[2,*] Wei-Chun Jao,[3,*] John P. Subasavage,[4,*] Joseph P. Chatelain,[5,*] Ken Slatten,[2] Adric R. Riedel,[6,*] Michele Silverstein,[3,*] and Matthew J. Payne[1]

[1] *Harvard-Smithsonian Center for Astrophysics, 60 Garden Street, Cambridge, MA 02138, USA*
[2] *RECONS Institute, Chambersburg, Pennsylvania, 17201*
[3] *Department of Physics and Astronomy, Georgia State University, Atlanta, GA 30302-4106*
[4] *The Aerospace Corporation, 2310 E. El Segundo Boulevard, El Segundo, CA 90245*
[5] *Las Cumbres Observatory, 6740 Cortona Dr., Suite 102, Goleta, CA 93117*
[6] *Space Telescope Science Institute, Baltimore, MD 21218*

ABSTRACT

We present results of the largest, most comprehensive study ever done of the stellar multiplicity of the most common stars in the Galaxy, the red dwarfs. We have conducted an all-sky survey for stellar companions to 1120 M dwarfs known to lie within 25 pc of the Sun via trigonometric parallaxes. In addition to a comprehensive literature search, stars were explored in new surveys for companions at separations of 2″ to 300″. A reconnaissance of wide companions to separations of 300″ was done via blinking SuperCOSMOS BRI images. Complementary $I-$band images obtained primarily at the CTIO/SMARTS 0.9m and the Lowell 42in telescopes were used to search the target stars for companions at separations of 2″ to 180″. Various astrometric and photometric methods were used to probe the inner 2″ to reveal close companions. We report the discovery of 20 new companions and identify 56 candidate multiple systems. In addition, new VRI photometry for 165 primaries and companions was obtained as part of the effort to characterize these nearby M dwarf systems.

We synthesize the results of the imaging surveys and the literature search to find a stellar multiplicity rate of 26.1 ± 1.4% for M dwarfs. There is a broad peak in the separation distribution of the companions at 20 AU, i.e., a distance similar to the scale of our outer Solar System, with a weak trend of smaller projected separations for lower mass primaries. This peak in the distribution is roughly one-half the distance found for solar-type stars. A hint that M dwarf multiplicity may be a function of tangential velocity is found, with faster moving, presumably older, stars found to be multiple somewhat less often. We calculate that stellar companions make up at least 17% of mass attributed to M dwarfs in the solar neighborhood, with roughly 9% of M dwarf mass hidden as unresolved companions. Finally, considering all M dwarf primaries and companions, we find that the mass distribution for M dwarfs increases to the end of the stellar main sequence.

Keywords: stars: binaries: general — stars: low mass — stars: statistics — solar neighborhood

Corresponding author: Jennifer G. Winters
jennifer.winters@cfa.harvard.edu

* Visiting Astronomer, Cerro Tololo Inter-American Observatory. CTIO is operated by AURA, Inc. under contract to the National Science Foundation.

1. INTRODUCTION

Much like people, stars arrange themselves in various configurations – singles, doubles, multiples, clusters, and great aggregations known as galaxies. Each of these collections is different, depending on the proximity of the members and the shared history and composition of the stars involved. Stellar multiples and their properties (e.g., separations, mass ratios, etc.) provide fundamental clues about the nature of star formation, the distribution of baryonic mass in the Universe, and the evolution of stellar systems over time. How stars are parceled into singles, doubles, and higher order multiples also provides clues about the angular momentum distribution in stellar systems and can constrain whether or not planets may be found in these systems (Raghavan et al. 2010; Wang et al. 2014; Winn & Fabrycky 2015; Kraus et al. 2016). Of all the populations in our Galaxy, the nearest stars provide the fundamental framework upon which stellar astrophysics is based because they contain the most easily studied representatives of their kinds. Because M dwarfs, often called "red dwarfs", dominate the nearby stellar population, accounting for roughly 75% of all stars (Henry et al. 2006), they are a critical sample to study in order to understand stellar multiplicity.

Companion searches have been done for M dwarfs during the past few decades, but until recently, most of the surveys have had inhomogeneous samples made up of on the order of 100 targets. Table 1 lists these previous efforts, with the survey presented in this work listed at the bottom for comparison. With samples of only a few hundred stars, our statistical understanding of the distribution of companions is quite weak, in particular when considering the many different types of M dwarfs, which span a factor of eight in mass (Benedict et al. 2016). In the largest survey of M dwarfs to date, Dhital et al. (2010) studied mid-K to mid-M dwarfs from the Sloan Digital Sky Survey that were not nearby and found primarily wide multiple systems, including white dwarf components in their analysis. In the next largest studies, only a fraction of the M dwarfs studied by Janson et al. (2012, 2014a) had trigonometric distances available, leading to a sample that was not volume-limited. Ward-Duong et al. (2015) had a volume-limited sample with trigonometric parallaxes from *Hipparcos* (Perryman et al. 1997, updated in van Leeuwen 2007), but the faint limit of *Hipparcos* ($V \sim 12$) prevented the inclusion of later M dwarf spectral types.[1]

[1] These final three studies were underway simultaneously with the study presented here.

Considering the significant percentage of all stars that M dwarfs comprise, a study with a large sample (i.e., more than 1000 systems) is vital in order to arrive at a conclusive understanding of red dwarf multiplicity, as well as to perform statistical analyses of the overall results, and on subsamples based on primary mass, metallicity, etc. For example, using a binomial distribution for error analysis, an expected multiplicity rate of 30% on samples of 10, 100, and 1000 stars, respectively, yields errors of 14.5%, 4.6%, and 1.4%, illustrating the importance of studying a large, well-defined sample of M dwarfs, preferably with at least 1000 stars.

Here we describe a search for stellar companions to 1120 nearby M dwarfs. For these M dwarf primaries[2] with trigonometric parallaxes placing them within 25 pc, an all-sky multiplicity search for stellar components at separations of 2″ to 300″ was undertaken. A reconnaissance for companions with separations of 5–300″ was done via the blinking of digitally scanned archival SuperCOSMOS *BRI* images, discussed in detail in §4.1. At separations of 2″ to 10″, the environs of these systems were probed for companions via $I-$band images obtained at telescopes located in both the northern and southern hemispheres, as outlined in §4.2. The Cerro Tololo Inter-American Observatory / Small and Moderate Aperture Research Telescope System (CTIO/SMARTS) 0.9m and 1.0m telescopes were utilized in the southern hemisphere, and the Lowell 42in and United States Naval Observatory (USNO) 40in telescopes were used in the northern hemisphere (see §4.2 for specifics on each telescope). In addition, indirect methods based on photometry were used to infer the presence of nearly equal magnitude companions at separations less than ∼2″ (§4.3). Finally, various subsets of the sample were searched for companions at subarcsecond separations using long-term astrometry at the CTIO/SMARTS 0.9m (§4.3.3) and *Hipparcos* reduction flags (§4.3.4). Because spectral type M is effectively the end of the stellar main sequence, the stellar companions revealed in this search are, by definition, M dwarfs, as well. We do not include brown dwarf companions to M dwarfs in the statistical results for this study, although they are identified.

In the interest of clarity, we first define a few terms. *Component* refers to any member of a multiple system.

[2] We refer to any collection of stars and their companion brown dwarfs and/or exoplanets as a system, including single M dwarfs not currently known to have any companions. Systems that contained a white dwarf component were excluded from the sample, as the white dwarf was previously the brighter and more massive primary.

Table 1. Previous M Dwarf Multiplicity Studies - Techniques

Reference	# of Stars	Technique	Search Region	MR	Notes
Skrutskie et al. (1989)	55	Infrared Imaging	2 — 14″	···	multiplicity not reported
Henry & McCarthy (1990)	27	Infrared Speckle	0.2 — 5″	34 ± 9	
Henry (1991)	74	Infrared Speckle	0.2 — 5″	20 ± 5	
Fischer & Marcy (1992)	28-62	Various	various	42 ± 9	varied sample
Simons et al. (1996)	63	Infrared Imaging	10 — 240″	40	
Delfosse et al. (1999a)	127	Radial Velocities	<1.0″	···	multiplicity not reported
Law et al. (2006)	32	Lucky Imaging	0.1 — 1.5″	7^{+7}_{-3}	M5 - M8
Endl et al. (2006)	90	Radial Velocities	<1.0″	···	Jovian search
Law et al. (2008)	77	Lucky Imaging	0.1 — 1.5″	$13.6^{+6.5}_{-4}$	late-type M's
Bergfors et al. (2010)	124	Lucky Imaging	0.2 — 5″	32 ± 6	young M0 - M6
Dhital et al. (2010)	1342	Sloan Archive Search	7 — 180″	···	wide binary search
Law et al. (2010)	36	Adaptive Optics	0.1 — 1.5″	···	wide binary search
Dieterich et al. (2012)	126	HST-NICMOS	0.2 — 7.5″	···	brown dwarf search
Janson et al. (2012)	701	Lucky Imaging	0.08 — 6″	27 ± 3	young M0 - M5
Janson et al. (2014a)	286	Lucky Imaging	0.1 — 5″	21-27	> M5
Ward-Duong et al. (2015)	245	Infrared AO	10 — 10,000 AU	23.5 ± 3.2	K7 - M6
This survey	1120	Various	0 — 300″	26.1 ± 1.4	all trig. distances

The *primary* is either a single star or the most massive (or brightest in V) component in the system, and *companion* is used throughout to refer to a member of a multiple system that is less massive (or fainter, again in V) than the primary star. Finally, we use the terms 'red dwarf' and 'M dwarf' interchangeably throughout.

2. DEFINITION OF THE SAMPLE

The 1120 systems in the survey sample have published trigonometric parallaxes, π_{trig}, of at least 40 mas with errors of 10 mas or less. All members of a system are assumed to have the same π_{trig} and proper motion, μ. In the cases of some widely separated binaries where separate parallaxes are available for each component, these are combined into a weighted mean. As shown in Table 2, there are three primary sources of trigonometric parallax data for M dwarfs currently available. The *General Catalogue of Trigonometric Stellar Parallaxes, Fourth Edition* (van Altena et al. 1995), often called the Yale Parallax Catalogue (hereafter YPC), is a valuable compendium of ground-based parallaxes published prior to 1995 and includes just under half of the nearby M dwarf parallaxes measured to date, primarily from parallax programs at the Allegheny, Mt. Stromlo, McCormick, Sproul, US Naval, Van Vleck, Yale, and Yerkes Observatories. The *Hipparcos* mission (initial release by Perryman et al. (1997), and revised results used here by van Leeuwen (2007); hereafter HIP) updated some of those parallaxes, and contributed 229 new systems for bright ($V \lesssim 12.5$) nearby M dwarfs. Overall, 743 systems have parallaxes from the YPC and HIP catalogs.

The next largest collection of parallaxes measured for nearby M dwarfs is from the RECONS[3] team, contributing 308 red dwarf systems to the 25 pc census via new measurements (Jao et al. 2005, 2011, 2014; Costa et al. 2005, 2006; Henry et al. 2006; Subasavage et al. 2009; Riedel et al. 2010, 2011, 2014; von Braun et al. 2011; Mamajek et al. 2013; Dieterich et al. 2014; Winters et al. 2017; Bartlett et al. 2017; Jao et al. 2017; Henry et al. 2018), published in *The Solar Neighborhood* series of papers (hereafter TSN) in *The Astronomical Journal*.[4] Finally, other groups have contributed parallaxes for an additional 70 nearby M dwarfs. As shown in Table 2, RECONS' work in the southern hemisphere creates a balanced all-sky sample of M dwarfs with known distances for the first time, as the southern hemisphere has historically been under-sampled. An important aspect of the sample surveyed here is that because all 1120 systems have accurate parallaxes, biases inherent to photometrically-selected samples are ameliorated. We note that for objects with parallaxes reported from multiple sources, we calculate a weighted mean parallax and parallax error.

A combination of color and absolute magnitude limits was used to select a sample of *bona fide* M dwarfs. Stars

[3] REsearch Consortium On Nearby Stars, *www.recons.org*

[4] A few unpublished measurements used in this study are scheduled for a forthcoming publication in this series.

Table 2. Parallax Sources for Multiplicity Search

Reference	# of Targets North of $\delta = 0$	# of Targets South of $\delta = 0$
YPC	389	124
HIP	83	146
RECONS - published	31	272
RECONS - unpublished	2	3
Literature (1995-2012)	52	18
TOTAL	557	564

Table 3. Astrometry Data

Name	R.A.	Decl.	μ ($''$yr^{-1})	P.A. (deg)	Ref	π (mas)	σ_π (mas)	# π	Ref
(1)	(2)	(3)	(4)	(5)	(6)	(7)	(8)	(9)	(10)
GJ 1001ABC	00 04 36.5	−40 44 03	1.636	159.7	71	77.90	2.04	2	15,68
GJ 1	00 05 24.4	−37 21 27	6.106	112.5	28	230.32	0.90	2	68,69
LHS 1019	00 06 19.2	−65 50 26	0.564	158.7	72	59.85	2.64	1	69
GJ 1002	00 06 43.2	−07 32 17	2.041	204.0	39	213.00	3.60	1	68
GJ 1003	00 07 26.7	+29 14 33	1.890	127.0	38	53.50	2.50	1	68
LHS 1022	00 07 59.1	+08 00 19	0.546	222.0	38	44.00	6.30	1	68
L 217-28	00 08 17.4	−57 05 53	0.370	264.0	40	75.17	2.11	1	73
HIP 687	00 08 27.2	+17 25 27	0.110	233.8	28	45.98	1.93	1	69
G 131-26AB	00 08 54.0	+20 50 18	0.251	194.4	53	54.13	1.35	1	53
GJ 7	00 09 04.3	−27 07 20	0.715	079.7	72	43.61	2.56	2	68,69
LEHPM 1-255	00 09 45.1	−42 01 40	0.271	096.7	72	53.26	1.51	1	73

NOTE—The first 10 lines of this Table are shown to illustrate its form and content.

[a] The weighted mean parallax includes the parallax of both the primary and the secondary components.

[b] The HIP parallax is markedly different from that published in YPC.

References— (1) Andrei et al. (2011); (2) Anglada-Escudé et al. (2012); (3) Bartlett et al. (2017); (4) Benedict et al. (1999); (5) Benedict et al. (2000); (6) Benedict et al. (2001); (7) Benedict et al. (2002); (8) Biller & Close (2007); (9) Costa et al. (2005); (10) Costa et al. (2006); (11) Dahn et al. (2002); (12) Deacon & Hambly (2001); (13) Deacon et al. (2005b); (14) Deacon et al. (2005a); (15) Dieterich et al. (2014); (16) Dupuy & Liu (2012); (17) Fabricius & Makarov (2000); (18) Faherty et al. (2012); (19) Falin & Mignard (1999); (20) Gatewood et al. (1993); (21) Gatewood et al. (2003); (22) Gatewood (2008); (23) Gatewood & Coban (2009); (24) Henry et al. (1997); (25) Henry et al. (2006); (26) Henry et al. (2018); (27) Hershey & Taff (1998); (28) Høg et al. (2000); (29) Ianna et al. (1996); (30) Jao et al. (2005); (31) Jao et al. (2011); (32) Jao et al. (2017); (33) Khovritchev et al. (2013); (34) Lèpine & Shara (2005); (35) Lèpine et al. (2009); (36) Lurie et al. (2014); (37) Luyten (1979a); (38) Luyten (1979b); (39) Luyten (1980a); (40) Luyten (1980b); (41) Martin & Mignard (1998); (42) Martinache et al. (2007); (43) Martinache et al. (2009); (44) Monet et al. (2003); (45) Pokorny et al. (2004); (46) Pourbaix et al. (2003); (47) Pravdo et al. (2006); (48) Pravdo & Shaklan (2009); (49) RECONS (in prep); (50) Reid et al. (2003); (51) Riedel et al. (2010); (52) Riedel et al. (2011); (53) Riedel et al. (2014); (54) Riedel et al. (2018); (55) Schilbach et al. (2009); (56) Schmidt et al. (2007); (57) Shakht (1997); (58) Shkolnik et al. (2012); (59) Smart et al. (2007); (60) Smart et al. (2010); (61) Söderhjelm (1999); (62) Subasavage et al. (2005a); (63) Subasavage et al. (2005b); (64) Teegarden et al. (2003); (65) Teixeira et al. (2009); (66) Tinney et al. (1995); (67) Tinney (1996); (68) van Altena et al. (1995); (69) van Leeuwen (2007); (70) von Braun et al. (2011); (71) Weis (1999); (72) Winters et al. (2015); (73) Winters et al. (2017).

within 25 pc were evaluated to define the meaning of "M dwarf" by plotting spectral types from RECONS (Riedel et al. 2014), Gray et al. (2003), Reid et al. (1995), and Hawley et al. (1996) versus $(V - K)$ and M_V. Because spectral types can be imprecise, there was overlap between the K and M types, so boundaries were chosen to split the types at carefully defined $(V - K)$ and M_V values. A similar method was followed for the M-L dwarf transition using results primarily from Dahn et al. (2002). These procedures resulted in ranges of $8.8 \leq M_V \leq 20.0$ and $3.7 \leq (V - K) \leq 9.5$ for stars we consider to be M dwarfs. For faint stars with no reliable V available, an initial constraint of $(I - K) \leq 4.5$ was also used to create the sample until V could be measured. These observational parameters correspond to masses of $0.63 < M_\odot < 0.075$, based on the mass-luminosity relation presented in Benedict et al. (2016).

Imposing these distance, absolute magnitude, and color criteria yields a sample of 1120 red dwarf primaries as of January 1, 2012, when the companion search observing program commenced. The astrometry data for these 1120 systems are listed in Table 3. Included are the names of the M dwarf primary, coordinates (J2000.0), proper motion magnitudes and position angles with references, the weighted means of the published trigonometric parallaxes and the errors, and the number of parallaxes included in the weighted mean and references. We note that for multiple systems, the proper motion of the primary component has been assumed to be the same for all members of the system. In the case of multiple systems for which parallax measurements exist for companions, as well as for the primaries, these measurements have been combined in the weighted means. All proper motions are from SuperCOSMOS, except where noted. Proper motions with the reference 'RECONS (in prep)' indicate SuperCOSMOS proper motions that will be published in the forthcoming RECONS 25 Parsec Database (Jao et al., in prep), as these values have not been presented previously. The five parallaxes noted as 'in prep' will be presented in upcoming papers in the TSN series.

3. $V_J R_{KC} I_{KC}$ PHOTOMETRY

As part of the effort to characterize the M dwarfs in the survey, new and published $V_J R_{KC} I_{KC}$[5] photometry were gathered and are presented in Table 4. Included are the names of the M dwarfs (column 1), the number of known components in the systems and in the photometry (2), J2000.0 coordinates (3, 4), VRI magnitudes (5, 6, 7), the number of observations and/or references (8), the 2MASS JHK_s magnitudes (9, 10, 11), and the photometric distance estimate. Next are listed the ΔV

[5] These subscripts will be dropped henceforth.

magnitudes between companions and primaries where needed (12), the deblended V magnitudes V_{db} (13), and estimated masses for each component (14).

Components of multiple systems are noted with a capital letter (A,B,C,D,E) after the name in the first column. If the names of the components are different, the letters identifying the primary and the secondary are placed within parentheses, e.g., LHS1104(A) and LHS1105(B). If the star is a companion in a multiple system, '0' is given in column (2). If a system has been resolved, numbers in parentheses next to the number of components indicates how many objects are included in the VRI photometry. For example, the notation '2(1)' indicates that the star is the primary in a binary and has individual photometry, whereas '0(1)' indicates that the star is a component of a multiple system for which separate photometry is available. An unresolved binary with blended photometry will be listed simply as '2' in the second column, and 'J' for joint photometry is listed with each blended magnitude. Brown dwarf companions are noted by a 'BD' next to the '0' in column 2, and often do not have complete, if any, VRI.

For new photometry reported here, superscripts are added to the references indicating which telescope(s) was used to acquire the VRI photometry: '09' for the CTIO/SMARTS 0.9m, '10' for the CTIO/SMARTS 1.0m, '40' for the USNO 40in, and '42' for the Lowell 42in. If the ΔV is larger than 3, the magnitude of the primary is treated as unaffected by the companion(s). All masses are estimated from the absolute V magnitude, which has been calculated from the deblended V magnitude for each star in column (13), the parallax in Table 3, and the empirical mass-luminosity relations of Benedict et al. (2016). If any type of assumption or conversion was made regarding the ΔV (as discussed in §7.1), the ΔV value, the V_{db} value, and the mass estimate are all shown in italics.

VRI photometry for many of the southern M dwarf primaries has been presented previously in Winters et al. (2011, 2015, 2017). New absolute photometry in the Johnson-Kron-Cousins VRI[6] filters for 95, 3, and 67 stars was acquired at the CTIO/SMARTS 0.9m, CTIO/SMARTS 1.0m, and Lowell 42in telescopes, respectively, and is presented here for the first time. Identical observational methods were used at all three sites. As in previous RECONS efforts, standard star fields from Graham (1982), Bessel (1990), and/or Landolt (1992, 2007, 2013) were observed multiple times each night to derive transformation equations and extinction curves. In order to match those used by Landolt, apertures 14″ in diameter were used to determine the stellar fluxes, except in cases where close contaminating sources needed to be deblended. In these cases, smaller apertures were used and aperture corrections were applied. Further details about the data reduction procedures, transformation equations, etc., can be found in Jao et al. (2005), Winters et al. (2011), and Winters et al. (2015).

In addition to the 0.9m, 1.0m, and 42in observations, three stars were observed at the United States Naval Observatory (USNO) Flagstaff Station 40in telescope. Basic calibration frames, bias and sky flats in each filter are taken either every night (bias) or over multiple nights in a run (sky flats) and are applied to the raw science data. Standard star fields from Landolt (2009, 2013) were observed at multiple airmasses between ∼1.0 and ∼2.1 each per night to calculate extinction curves. All instrumental magnitudes, both for standards and science targets, are extracted by fitting spatially-dependent point spread functions (PSFs) for each frame using Source Extractor (*SExtractor* (Bertin & Arnouts 1996) and *PSFEx* (Bertin 2011), with an aperture diameter of 14″. Extensive comparisons of this technique to basic aperture photometry have produced consistent results in uncrowded fields.

As outlined in Winters et al. (2011), photometric errors at the 0.9m are typically 0.03 mag in V and 0.02 mag in R and I. To verify the Lowell 42in data[7], Table 5 presents photometry for four stars observed at the Lowell 42in and at the CTIO/SMARTS 0.9m, as well as six additional stars with VRI from the literature. Results from the 42in and 0.9m match to 0.06 mag, except for the R magnitude of GJ 1167, which can be attributed to a possible flare event observed at the time of observation at the 42in, as the V and I magnitudes are consistent. This object is, in fact, included in a flare star catalog of UV Cet-type variables (Gershberg et al. 1999). An additional six stars were observed by Weis[8], and the photometry matches to within 0.08 mag for all six objects, and typically to 0.03 mag. Given our typical 1σ errors of at most 0.03 mag for VRI, we find that the Lowell 42in data have differences of 2σ or less in 28 of the 30 cases shown in Table 5.

[6] The central wavelengths for the V_J, R_{KC}, and I_{KC} filters at the 0.9m are 5438Å, 6425Å, and 8075Å, respectively; filters at other telescopes are similar.

[7] No rigorous comparisons are yet possible for our sample of red dwarfs for the CTIO/SMARTS 1.0m and USNO 40in, given only three stars observed at each.

[8] All photometry from Weis has been converted to the Johnson-Kron-Cousins (JKC) system.

Table 4. Photometry Data

Name	# Obj	R.A.	Decl.	V_J	R_{KC}	I_{KC}	# nts/ref	J	H	K_s	π_{ccd}	σ_π	ΔV	V_{db}	Mass
				(mag)	(mag)	(mag)		(mag)	(mag)	(pc)	(pc)	(mag)	(mag)	($M_\odot$)	
(1)	(2)	(3)	(4)	(5)	(6)	(7)	(8)	(9)	(10)	(11)	(12)	(13)	(14)	(15)	(16)
GJ 1001C	0BD	00 04 34.8	−40 44 06	...	...	...	...	...	...	...	...	...	...	...	...
GJ 1001BC	0BD	00 04 34.8	−40 44 06	22.77J	19.24J	16.76J	/9	13.11J	12.06J	11.40J	...	...	...	...	...
GJ 1001A	3(1)	00 04 36.5	−40 44 03	12.83	11.62	10.08	/40	8.60	8.04	7.74	12.5	1.9	...	12.83	0.23
GJ 1	1	00 05 24.4	−37 21 27	8.54	7.57	6.41	/2	5.33	4.83[a]	4.52	5.6	0.9	...	8.54	0.41
LHS 1019	1	00 06 19.2	−65 50 26	12.17	11.11	9.78	/17	8.48	7.84	7.63	16.6	2.6	...	12.17	0.34
GJ 1002	1	00 06 43.2	−07 32 17	13.84	12.21	10.21	/33	8.32	7.79	7.44	5.4	1.0	...	13.84	0.12
GJ 1003	1	00 07 26.7	+29 14 33	14.16	13.01	11.54	/30	10.22	9.74	9.46	36.0	7.0	...	14.16	0.20
LHS 1022	1	00 07 59.1	+08 00 19	13.09	12.02	10.65	/30	9.39	8.91	8.65	28.9	5.2	...	13.09	0.31
L 217-28	1	00 08 17.4	−57 05 53	12.13	11.00	9.57	/33	8.21	7.63	7.40	13.2	2.0	...	12.13	0.29
HIP 687	1	00 08 27.2	+17 25 27	10.80	9.88	8.93	/28	7.81	7.17	6.98	18.5	3.2	...	10.80	0.58

NOTE—The first 10 lines of this Table are shown to illustrate its form and content.

NOTE—A 'J' next to a photometry value indicates that the magnitude is blended due to one or more close companions.

[a] $2MASS$ magnitude error greater than 0.05 mags.

References—(1) this work; (2) Bessel (1990); (3) Bessell (1991); (4) Costa & Méndez (2003); (5) Costa et al. (2005); (6) Costa et al. (2006); (7) Dahn et al. (1982); (8) Dahn et al. (2002); (9) Dieterich et al. (2014); (10) Harrington & Dahn (1980); (11) Harrington et al. (1993); (12) Henry et al. (2004); (13) Henry et al. (2006); (14) Høg et al. (2000); (15) Jao et al. (2005); (16) Jao et al. (2011); (17) Jao et al. (2014); (18) Kilkenny et al. (2007); (19) Koen et al. (2002); (20) Koen et al. (2010); (21) Lèpine et al. (2009); (22) Patterson et al. (1998); (23) Reid et al. (2002); (24) Reid et al. (2003); (25) Reid et al. (2004); (26) Riedel et al. (2010); (27) Riedel et al. (2014); (28) Weis & Upgren (1982); (29) Weis (1984); (30) Weis (1986); (31) Weis (1987); (32) Weis (1988); (33) Weis (1991a); (34) Weis (1991b); (35) Weis (1993); (36) Weis (1994); (37) Weis (1996); (38) Weis (1999); (39) Winters et al. (2011); (40) Winters et al. (2015); (41) Winters et al. (2017).

Table 5. Overlapping Photometry Data

Name	$(V-K)$	V_J	R_{KC}	I_{KC}	# obs	tel/ref
	(mag)	(mag)	(mag)	(mag)		
2MA 0738+2400	4.86	12.98	11.81	10.35	1	42in
		12.98	11.83	10.35	2	0.9m
G 43-002	4.76	13.23	12.08	10.67	1	42in
		13.24	12.07	10.66	2	0.9m
2MA 1113+1025	5.34	14.55	13.27	11.63	1	42in
		14.50	13.21	11.59	2	0.9m
GJ 1167	5.59	14.16	12.67	11.10	1	42in
		14.20	12.82	11.11	1	0.9m
LTT 17095A	4.22	11.12	10.12	9.00	1	42in
		11.11	10.11	8.94	...	1
GJ 15B	5.12	11.07	9.82	8.34	2	42in
		11.06	9.83	8.26	...	3
GJ 507AC	3.96	9.52	8.56	7.55	1	42in
		9.52	8.58	7.55	...	3
GJ 507B	4.64	12.15	11.06	9.66	1	42in
		12.12	11.03	9.65	...	3
GJ 617A	3.64	8.59	7.68	6.85	1	42in
		8.60	7.72	6.86	...	3
GJ 617B	4.67	10.74	9.67	8.29	1	42in
		10.71	9.63	8.25	...	2

References—(1) Weis (1993); (2) Weis (1994); (3) Weis (1996).

4. THE SEARCHES

Several searches were carried out on the 1120 nearby M dwarfs in an effort to make this the most comprehensive investigation of multiplicity ever undertaken for stars that dominate the solar neighborhood. Information about the surveys is collected in Tables 6–12, including a statistical overview of the individual surveys in Table 6, specifics about the Blink Survey in Table 7 and telescopes used for the CCD Imaging Survey in Table 8. Detection limit information for the CCD Imaging Survey is presented in Tables 9 and 10. Results for confirmed multiples are collected in Table 11, whereas candidate, but as yet unconfirmed, companions are listed in Table 12.

4.1. *Wide-Field Blinking Survey: Companions at 5–300″*

Because most nearby stars have large proper motions, images of the stars taken at different epochs were blinked for common proper motion (CPM) companions with separations of 5–300″.[9] A wide companion would have a similar proper motion to its primary and would thus appear to move in the same direction at the same speed

[9] In this study, only two companions, the tertiaries LHS1521C and G164-049C, are found further than 300″ from an M dwarf primary, at separations of 1164″ and 4343″, respectively.

Table 6. Companion Search Technique Statistics

Technique	Separation	Searched	Searched	Detected
	(″)	(#)	(%)	(#)
Image Blinking	10–300	1110	99	64
CCD Imaging	2–10	1120	100	44
HR Diagram Elevation	< 2	1120	100	10
Distance Mismatches	< 2	1112	99	37
RECONS Perturbations	< 2	324	29	39
Hipparcos Flags	< 2	460	41	31
Literature/WDS Search	all	1120	100	292
Individual companions	TOTAL	1120	100	312

Table 7. Blink Survey Information

Filter	Epoch Span	DEC Range	Mag. Limit	$\Delta\lambda$
	(yr)	(deg)	(mag)	(Å)
B_J (IIIaJ)	1974 - 1994	all-sky	∼20.5	3950 - 5400
R_{59F} (IIIaF)	1984 - 2001	all-sky	∼21.5	5900 - 6900
I_{IVN} (IVN)	1978 - 2002	all-sky	∼19.5	6700 - 9000
E_{POSS-I} (103aE)	1950 - 1957	$-20.5 < \delta < +05$	∼19.5	6200 - 6700
I_{KC}	2010 - 2014	all sky	∼17.5	7150 - 9000

across the sky. Archival SuperCOMOS $B_J R_{59F} I_{IVN}$[10] photographic plate images $10' \times 10'$ in size were blinked using the Aladin interface of the Centre de Donneès astronomiques de Strasbourg (CDS) to detect companions at separations greater than ∼5″. These plates were taken from 1974–2002 and provide up to 28 years of temporal coverage, with typical epoch spreads of at least 10 years. Information for the images blinked is given in Table 7, taken from Morgan (1995), Subasavage (2007), and the UK Schmidt webpage.[11] Candidates were confirmed to be real by collecting VRI photometry and estimating photometric distances using the suite of relations in Henry et al. (2004); if the distances of the primary and candidate matched to within the errors on the distances, the candidate was deemed to be a physical companion.

4.1.1. *Blink Survey Detection Limits*

[10] These subscripts will be dropped henceforth.
[11] *http://www.roe.ac.uk/ifa/wfau/ukstu/telescope.html*

The CPM search had two elements that needed to be evaluated in order to confidently identify objects moving with the primary star in question: companion brightness and the size of each system's proper motion.

A companion would have to be detectable on at least two of the three photographic plates in order to notice its proper motion, so any companion would need to be brighter than the magnitude limits given in Table 7 in at least two images. Because the search is for *stellar* companions, it is only necessary to be able to detect a companion as faint as the faintest star in the sample, effectively spectral type M9.5 V at 25 pc. The two faintest stars in the sample are DEN 0909-0658, with VRI = 21.55, 19.46, 17.18 and RG0050-2722 with VRI = 21.54, 19.09, 16.65. The B magnitudes for these stars are both fainter than the mag∼20.5 limit of the B plate, and thus neither star was detected in the B image; however, their R and I magnitudes are both brighter than the limits of those plates and the stars were identified in both the R and I images. Ten other objects are too faint to be seen on the B plate, but as is the case with DEN0909-0658 and RG0050-2722, all are bright enough for detection in the R and I images.

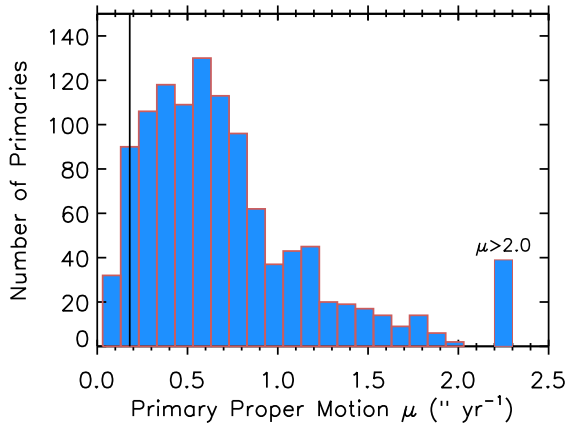

Figure 1. Histogram of the proper motion of the primary (or single) component in each system is plotted, with the vertical line indicating $\mu = 0''.18$ yr^{-1}, the canonical lower proper motion limit of Luyten's surveys. Because these systems are all within 25 pc, the majority (95%) have proper motions, μ, larger than $0''.18$ yr^{-1}.

Even though all stellar companions should be bright enough to be in at least two of the SuperCOSMOS images, the epoch spread between the plates needed to be large enough to detect the primary star moving in order to then notice a companion moving in tandem with it. As shown in the histogram of proper motions in Figure 1, most of the survey stars move faster than $0''.18$ yr^{-1}, the historical cutoff of Luyten's proper motion surveys.

Hence, even a 10-year baseline provides 1.″8 of motion, easily discerned when blinking plates. However, 58 of the stars in the survey (∼5% of the sample) have $\mu < 0.''18$ yr^{-1}, down to the slowest star with $\mu = 0.''03$ yr^{-1}; for this star, to detect a motion of 1.″8 the epoch spread would need to be 60 years. For 18 stars with Decl $-20 < \delta < +5°$, the older POSS-I plate (taken during 1950–1957) was used for the slow-moving primaries. This extended the epoch spread by 8–24 years, enabling companions for these 18 stars to be detected, leaving 40 slow-moving stars to search.

The proper motions of 151 more primaries were not able to confidently be detected because the epoch spread of the SuperCOSMOS plates was less than 5 years. These 151 stars, in addition to the 40 stars with low μ mentioned above that were not able to be blinked using the POSS plates, were compared to our newly-acquired $I-$band images taken during the CCD Imaging Survey, extending the epoch spread by almost twenty years in some cases. Wherever possible, the SuperCOSMOS $I-$band image was blinked with our CCD $I-$band image, but sometimes a larger epoch spread was possible with either the $B-$ or $R-$band plate images. In these cases, the plate that provided the largest epoch spread was used. In order to upload these images to *Aladin* to blink with the archival SuperCOSMOS images, World Coordinate System (WCS) coordinates were added to the header of each image so that the two images could be aligned properly. This was done using *SExtractor* for the CTIO/SMARTS 0.9m and the USNO 40in images and Astrometry.net for the Lowell 42in and the CTIO/SMARTS 1.0m images. One new candidate companion with similar proper motion was identified: 2MA0936-2610B.

After using the various techniques outlined above to extend the image epoch spreads, 1110 of 1120 stars were sucessfully searched in the Blink Survey for companions. In ten cases, either the primary star's proper motion was still undetectable, the available CCD images were taken under poor sky conditions and many faint sources were not visible, or the frame rotations converged poorly. A primary result from this Blink Survey is that in the separation regime from 10–300″, where the search is effectively complete, we find a multiplicity rate of 4.6% (as discussed in §6). Thus, we estimate that only 0.5 CPM stellar companions (10 ∗ 4.6%) with separations 10–300″ were missed due to not searching 10 stars for wide companions.

4.2. *CCD Imaging Survey: Companions at 2–10″*

To search for companions with separations 2–10″, astrometry data were obtained at four different telescopes:

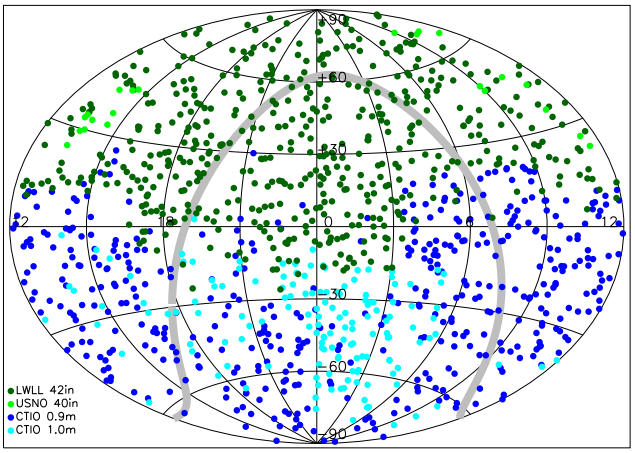

Figure 2. The distribution on the sky of all 1120 M dwarfs examined for multiplicity. Illustrated is the uniformity of the sample in both hemispheres, due in large part to RECONS' parallax work in the southern hemisphere. Different colors indicate the different telescopes that were utilized for the CCD imaging search: royal blue for the CTIO/SMARTS 0.9m, dark green for the Lowell 42in, cyan for the CTIO/SMARTS 1.0m, and bright green for the USNO 40in. The Galactic plane is outlined in gray.

Table 8. Telescopes Utilized for CCD Imaging Search and VRI Photometry

Telescope	FOV	Pixel Scale	# Nights	# Objects
Lowell 42in	22.3′ × 22.3′	0.″327 px^{-1}	21	508
USNO 40in	22.9′ × 22.9′	0.″670 px^{-1}	1	22
CTIO/SMARTS 0.9m	13.6′ × 13.6′	0.″401 px^{-1}	16	442
CTIO/SMARTS 1.0m	19.6′ × 19.6′	0.″289 px^{-1}	8	148

in the northern hemisphere, the Hall 42in telescope at Lowell Observatory and the USNO 40in telescope, both in Flagstaff, AZ, and in the southern hemisphere, the CTIO/SMARTS 0.9m and 1.0m telescopes, both at Cerro Tololo Inter-American Observatory in Chile. Figure 2 shows the distribution on the sky of the entire sample investigated for multiplicity. The different colors indicate the different telescopes used during this CCD imaging campaign. Note the balance in the distribution of stars surveyed, with nearly equal numbers of M dwarfs in the northern and southern skies.

Technical details for the cameras and specifics about the observational setups and numbers of nights and stars observed at each telescope are given in Table 8. The telescopes used for the imaging campaign all have primaries ∼1m in size and have CCD cameras that provide similar

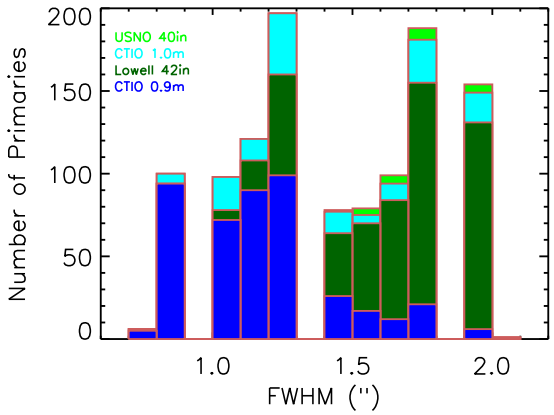

Figure 3. The seeing FWHM measured for target star frames used in the $I-$band CCD imaging search. The four different telescopes used are represented as royal blue for the CTIO/SMARTS 0.9m, dark green for the Lowell 42in, cyan for the CTIO/SMARTS 1.0m, and bright green for the USNO 40in. Note the generally superior seeing conditions for targets observed at the 0.9m.

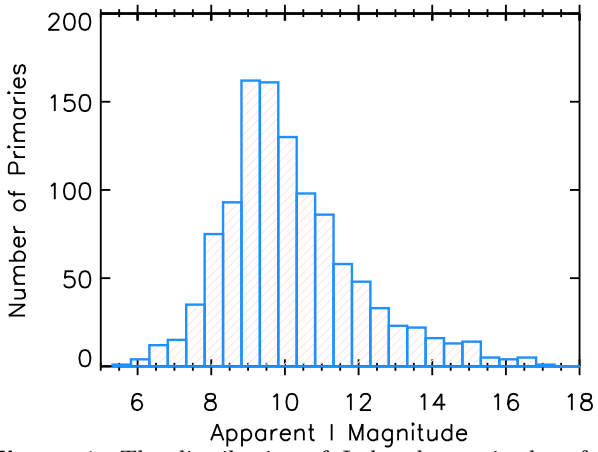

Figure 4. The distribution of $I-$band magnitudes of our sample of 1120 M dwarfs known to lie within 25 pc, illustrating that most (85%) of the target stars are brighter than I = 12.

pixel scales: images have 0.″327 per pixel at the Lowell 42in, 0.″670 per pixel at the USNO 40in, 0.″401 per pixel at the CTIO/SMARTS 0.9m, and 0.″289 per pixel at the CTIO/SMARTS 1.0m. Data from all telescopes were acquired without binning pixels. The histogram in Figure 3 illustrates the seeing measured for the best images of each star surveyed at the four different telescopes. Seeing conditions better than 2″ were attained for all but one star, GJ 507, with some stars being observed multiple times. While the 0.9m has a slightly larger pixel scale than the 1.0m and the 42in, as shown in Figure 3, the seeing was typically better at that site, allowing for better resolution. Only 22 primaries (fewer than 2% of the survey) were observed at the USNO 40in, so we do not consider the coarser pixel scale to have significantly affected the survey. Overall, the data from the four telescopes used were of similar quality and the results could be combined without modification.

A few additional details of the observations are worthy of note:

• A total of 444 stars were observed at the CTIO/SMARTS 0.9m telescope, where consistently good seeing, telescope operation, and weather conditions make observations at this site superior to those at the other telescopes used, as illustrated in Figure 3.

• While being re-aluminized in December 2012, the primary mirror at the Lowell 42in was dropped and damaged. The cardboard mask that was installed over the damaged mirror as a temporary fix resulted in a PSF flare before a better mask was installed that slightly improved the PSF. Of the 509 stars observed for astrometry at Lowell, 458 were observed before the mishap and 51 after.

• $I-$band images at both the Lowell 42in and CTIO/SMARTS 1.0m suffer from fringing, the major cause of which is night sky emission from atmospheric OH molecules. This effect sometimes occurs with back-illuminated CCDs at optical wavelengths longer than ∼700 nm where the light is reflected several times between the internal front and back surfaces of the CCD, creating constructive and destructive interference patterns, or fringing (Howell 2000, 2012). In order to remove these fringes, $I-$band frames from multiple nights with a minimum of saturated stars in the frame were selected, boxcar smoothed, and then average-combined into a fringe map. This fringe map was then subtracted from all $I-$band images using a modified IDL code originally crafted by Snodgrass & Carry (2013).

Figure 4 shows the distribution of the apparent I magnitudes of the red dwarfs surveyed, with a peak at I = 8.5–9.5. Each M dwarf primary was observed in the I_{KC} filter with integrations of 3, 30, and 300 seconds in order to reveal stellar companions at separations 2–10″. This observational strategy was adopted to reveal any close equal-magnitude companions with the short 3-second exposures, while the long 300-second exposures would reveal faint companions with masses at the end of the main sequence. The 30-second exposures were taken to bridge the intermediate phase space. Details about limitations of the search technique are given in §4.2.2. Calibration frames taken at the beginning of each night were used for typical bias subtraction and dome flat-fielding using standard *IRAF* procedures. Four new

companions were discovered during this portion of the survey.

4.2.1. *New Companions*

Several new companions were discovered during the surveys, or confirmed after being noticed during the long-term astrometry program at the CTIO/SMARTS 0.9m. In each case, archival plates were checked to eliminate the possibility that new companions were background objects.

• **GJ 84.1C (0205−2804)** was found as a nearly equal-magnitude companion separated by 1.5″ from GJ 84.1B at a position angle of 113 and with a $\Delta I = 0$ mag, making the system a triple.

• **2MA 0936-2610C (0936−2610)** We report the discovery of a new companion to this previously known double star at $\rho = 41.8''$, $\theta = 315°$, making this a triple system. The ΔV is 6.9 mag. The photographic distance for this new 'C' component estimated using SuperCOSMOS BRI plate magnitudes in combination with 2MASS JHK magnitudes is 16.8 ± 5.5 pc, while the distance estimate from our own $VRI + JHK$ photometry is 17.0 ± 2.8 pc. Both distances agree with the trigonometric distance for the AB components (18.6 ± 0.5 pc) within the errors.

• **UPM 1710-5300B (1710−5300)** was found as a companion separated by 1.3″ from its primary at a position angle of 110°, with $\Delta I = 2.0$ mag.

• **LHS 5348 (1927−2811)** This binary system discovery was previously reported in Winters et al. (2017) along with its parallax measurement; however, we include it here with updated multiplicity information, as it was discovered during the multiplicity survey. It is separated by 1″ from its primary at a position angle of 176°, with $\Delta I = 2.0$ mag.

• **2MA 1951-3510B (1951−3510)** was found as a companion separated by 1.6″ from its primary at a position angle of 125°, with $\Delta I = 1.0$ mag.

4.2.2. *CCD Imaging Survey Detection Limits*

An analysis of the detection limits of the CCD imaging campaign was done for objects with a range of I magnitudes at $\rho = 1$–5″ and at Δmags = 0 to 10 in one-magnitude increments for different seeing conditions at the two main telescopes where the bulk (85%) of the stars were imaged: the CTIO/SMARTS 0.9m and the Lowell 42in. The companion search in the CCD frames extended out to 10″, where sources were detected even more easily than at 5″.

Because the apparent $I-$band magnitudes for the stars in the sample range from 5.32–17.18 (as shown in Figure 4), objects with $I-$band magnitudes of approximately 8, 12, and 16 were selected for investigation.

Table 9. Stars Used for Detection Limit Study

Name	I (mag)	FWHM (arcsec)	Tel	Note
GJ 285	8.24	0.8	0.9m	
LP 848-050AB	12.47J	0.8	0.9m	ρ_{AB} <2″
SIP 1632-0631	15.56	0.8	0.9m	
L 032-009A	8.04	1.0	0.9m	ρ_{AB} = 22.″40
SCR 0754-3809	11.98	1.0	0.9m	
BRI 1222-1221	15.59	1.0	0.9m	
GJ 709	8.41	1.0	42in	
GJ 1231	12.08	1.0	42in	
Reference Star	16 (scaled)	1.0	42in	
GJ 2060AB	7.83J	1.5	0.9m	ρ_{AB} = 0.″485
2MA 2053-0133	12.46	1.5	0.9m	
Reference Star	16 (scaled)	1.5	0.9m	
GJ 109	8.10	1.5	42in	
LHS 1378	12.09	1.5	42in	
2MA 0352+0210	16.12	1.5	42in	
Reference Star	8 (scaled)	1.8	0.9m	
SCR 2307-8452	12.00	1.8	0.9m	
Reference Star	16 (scaled)	1.8	0.9m	
GJ 134	8.21	1.8	42in	
LHS 1375	12.01	1.8	42in	
SIP 0320-0446AB	16.37	1.8	42in	ρ_{AB} <0.″33
GJ 720A	8.02	2.0	42in	ρ_{AB} = 112.″10
LHS 3005	11.99	2.0	42in	
2MA 1731+2721	15.50	2.0	42in	

Only 88 primaries (7.8% of the sample) have $I < 8$, so it was not felt necessary to create a separate set of simulations for these brighter stars. The stars used for the detection limit analysis are listed in Table 9 with their I magnitudes, the FWHM at which they were observed and at which telescope, and any relevant notes.

As noted previously, the faintest primary in the $I-$band found in the sample is DEN 0909-0658 (I = 17.18), with $\pi = 42.5$ mas (corresponding to 23.5 pc), $(V - K) = 8.9$, and $M_V = 19.58$, all parameters that place it at the boundary of the sample in both distance and spectral type. Therefore, Δmags of up to 10 magnitudes were probed in order to determine if a companion with $I = 18$ could be detected within 1–5″ of a primary with $I = 8$.

Each of the selected test stars was analyzed in seeing conditions of 1.″0, 1.″5, and 1.″8, but because the seeing at CTIO is typically better than that at Anderson Mesa, we were able to push to 0.″8 for the 0.9m, and had to extend to 2.″0 for the Lowell 42in. These test stars were verified to have no known detectable companions within

the 1–5″ separations explored in this part of the project. We note that one of the targets examined for the best resolution test, LP 848-050AB, has an astrometric perturbation due to an unseen companion at an unknown separation, but that at FWHM of 0.8″, the two objects were still not resolved. As the imaging search probes separations 1–5″, using this star does not affect the detection limit analysis. The other binaries used all had either larger or smaller separations than the 1–5″ regions explored, effectively making them point sources.

The *IDL* SHIFT task was used to shift and add the science star as a proxy for an embedded companion, scaled by a factor of 2.512 for each magnitude difference. In cases where the science star was saturated in the frame, a reference star was selected from the shorter exposure taken in similar seeing in which the science star was not saturated. Its relative magnitude difference was calculated so that it could be scaled to the desired brightness in the longer exposure, and then it was embedded for the analysis. In all cases, the background sky counts were subtracted before any scaling was done.

Stars with $I = 8$ were searched for companion sources in *IRAF* via radial and contour plots using the 3-second exposure to probe ΔI = 0, 1, 2, 3, the 30-second exposure for ΔI = 4, 5, and the 300-second exposure for ΔI = 6, 7, 8, 9, 10. Similarly, twelfth magnitude stars were probed at ΔI = 0, 1, 2, 3 using the 30-second exposure and at ΔI = 4, 5 with the 300-second frame. Finally, the 300-second exposure was used to explore the regions around the sixteenth magnitude objects for evidence of a stellar companion at ΔI = 0, 1, 2.

In total, 800 contour plots were made using *IDL* and inspected by eye. A subset of 100 example plots for stars with I = 8.04, 11.98, and 15.59 observed in seeing conditions of 1.″0 at the 0.9m are shown in Figures 5 - 7. The 'Y', 'N', and 'M' labels in each plot indicate *yes*, *no*, or *maybe* for whether or not the injected synthetic companion was detectable by eye at the separation, magnitude, and seeing conditions explored. As can be seen, the I = 8.04 target star is highly saturated in the frames used for ΔI greater than 4. Overall, the companion can be detected in 72 of the 100 simulations, possibly detected in seven more cases, and not detected in twenty-one cases. The conditions in which the companion remains undetected are at small ρ, at $\Delta I > 4$, and at all ρ for ΔI = 10. Note that these images do not stand alone — contour plots for target stars are also compared to plots for other stars in the frames, allowing an additional check to determine whether or not the star in question is multiple.

The full range of ΔI for the M dwarf sequence is slightly less than nine magnitudes, so ΔI = 10 represents detections of brown dwarf companions. There were no companions detected with ΔI = 10 around the brighter stars in the simulations, indicating that this survey was *not* sensitive to brown dwarf companions at separations 1–5″ around the brightest M dwarfs in the sample, although they would be detected around many of the fainter stars (none were found). Because our search was for stellar companions, we can then ignore the ΔI = 10 results for our summary of detection sensitivity, reducing the total contour plot number to 760; these non-detections in the ΔI = 10 simulations are not included in Table 10 or in our summary.

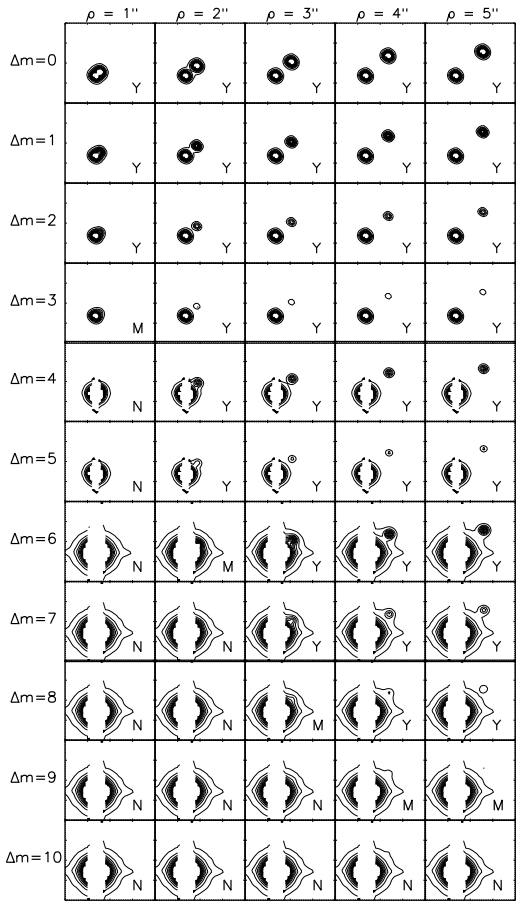

Figure 5. Detection Limits for the CTIO/SMARTS 0.9m: Contour plots for L 032-009A, with I = 8.04 in 1.″0 seeing conditions for an embedded companion at ρ = 1–5″ with Δmags = 0–10. The Y, N, and M labels indicate *yes*, *no*, or *maybe* for whether or not the embedded companion is detectable. The 3-second exposure was used for Δmags = 0–3, the 30-second exposure was used for Δmags = 4–5, and the 300-second exposure was used for Δmags = 6–10. Thirty-five simulated companions were detected, five were possibly detected, and 15 were undetectable.

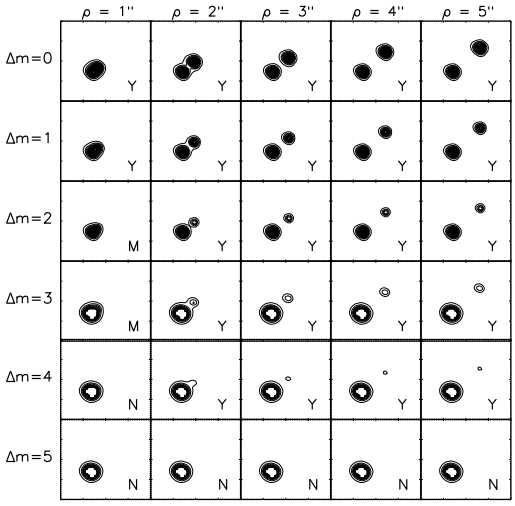

Figure 6. Detection Limits for the CTIO/SMARTS 0.9m: Contour plots for SCR 0754-3809, with $I = 11.98$ at $1\farcs0$ seeing conditions for an embedded companion at $\rho = 1{-}5''$ with Δmags = 0–5. The Y, N, and M labels indicate *yes*, *no*, or *maybe* for whether or not the embedded companion is detectable. The 30-second exposure was used for Δmags = 0, 1, 2, and the 300-second exposure was used for Δmags = 3, 4, 5. Twenty-two simulated companions were detected, two were possibly detected, and six were undetectable.

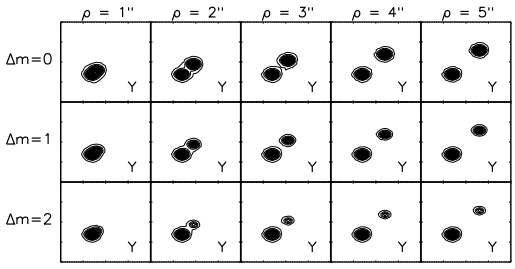

Figure 7. Detection Limits for the CTIO/SMARTS 0.9m: Contour plots for BRI 1222-1221, with $I = 15.59$ at $1\farcs0$ seeing conditions for an embedded companion at $\rho = 1{-}5''$ with Δmags = 0–2. The Y, N, and M labels indicate *yes*, *no*, or *maybe* for whether or not the embedded companion is detectable. The 300-second exposure was used. All 15 simulated companions were detected.

Table 10 presents a summary of the results of the detections of the embedded companions. Overall, the simulated companions were detected 68% of the time for all brightness ratios on both telescopes, were possibly detected in 9% of the simulations, and were not detected 23% of the time. For the simulations of bright stars with $I = 8$, 63% of the embedded companions were detected. For stars with $I = 12$, companions were detected in 66% of the time, and for the faint stars with $I = 16$, companions were detected in 89% of the cases tested. At $\rho = 1''$, embedded companions were detected in 27% of cases, possibly detected in 20% of cases, and not detected in 53% of cases. Thus, we do not claim high sensitivity at separations this small. At $\rho = 2''$, the percentages are 68%, 1%, and 22% for the 'yes', 'maybe', and 'no' cases, respectively. The detection rates are 80%, 8%, and 13% at $\rho = 3''$, 83%, 5%, 13% at $\rho = 4''$, and 83%, 3%, 14% at $\rho = 5''$.

Table 10. Detection Limit Summary

Seeing	Yes	No	Maybe	Yes	No	Maybe
Conditions	(#)	(#)	(#)	(#)	(#)	(#)
		0.9m			42in	
FWHM = $0\farcs8$	75	5	15	...	...	...
$I = 8$ mag	36	5	9	...	...	...
$I = 12$ mag	24	...	6	...	...	...
$I = 16$ mag	15	...	...	...	...	...
FWHM = $1\farcs0$	72	7	16	70	4	21
$I = 8$ mag	35	5	10	34	4	12
$I = 12$ mag	22	2	6	21	...	9
$I = 16$ mag	15	...	...	15	...	...
FWHM = $1\farcs5$	65	11	19	64	10	21
$I = 8$ mag	33	5	12	33	6	11
$I = 12$ mag	20	3	7	17	3	10
$I = 16$ mag	12	3	...	14	1	...
FWHM = $1\farcs8$	58	10	27	60	11	24
$I = 8$ mag	28	4	18	29	6	15
$I = 12$ mag	18	3	9	19	2	9
$I = 16$ mag	12	3	...	12	3	...
FWHM = $2\farcs0$	...	...	...	54	12	29
$I = 8$ mag	...	...	...	24	9	17
$I = 12$ mag	...	...	...	18	2	10
$I = 16$ mag	...	...	...	12	1	2
TOTAL	270	33	77	248	37	95

Figure 8 illustrates detected companions in the Blinking and CCD Imaging Surveys, providing a comparison for the detection limits derived here. We note that the largest ΔI detected was ~ 6.4 (GJ 184B), while the largest angular separation detected was $295''$ (GJ 49B). Four companions have angular separations outside the range of the plot, but within the $300''$ sensitivity of the searches. The two companions with the largest separations from their primaries - G 164-42C and GJ 130.1C - were not able to be confirmed during the blinking search, as their separations were larger than the field of view.

4.3. *Searches at Separations* $\leq 2''$

In addition to the blinking and CCD imaging searches, investigations for companions at separations smaller than $2''$ were possible using a variety of techniques, detailed next in Sections §4.3.1–4.3.4. Accurate parallaxes for all stars and $VRIJHK$ photometry for most stars were used to identify overluminous red dwarfs likely har-

Table 11. Multiplicity Information for Sample

Name	# Obj	Map	RA	DEC	ρ	θ	Year	Technique	Ref	Δmag	Filter	Ref
			(hh:mm:ss)	(dd:mm:ss)	($''$)	(deg)				(mag)		
GJ1001	0	BC	00 04 34.8	−40 44 06	0.087	048	2003	HSTACS	41	0.10	110	41
GJ1001	3	A-BC	00 04 36.0	−40 44 02	18.2	259	2003	visdet	41	9.91	V	1
G131-026	2	AB	00 08 54.0	+20 50 18	0.111	170	2001	AO det	13	0.46	H	13
GJ0011	2	AB	00 13 15.8	+69 19 36	0.859	089	2012	lkydet	63	0.69	i'	63
LTT17095	2	AB	00 13 38.7	+80 39 56	12.78	126	2001	visdet	107	3.63	V	1
GJ1005	2	AB	00 15 28.1	−16 08 01	0.329	234	2002	HSTNIC	31	2.42	V	9
2MA0015-1636	2	AB	00 15 58.1	−16 36 57	0.105	090	2011	AO det	18	0.06	H	18
L290-072	2	AB	00 16 01.9	−48 15 39	<1	...	2009	SB1	121	...	...	...
GJ1006	2	AB	00 16 14.6	+19 51 37	25.09	059	1999	visdet	107	0.94	V	116
GJ0015	2	AB	00 18 23.0	+44 01 24	35.15	064	1999	visdet	107	2.97	V	1

Note—The first 10 lines of this Table are shown to illustrate its form and content.

Note—The codes for the techniques and instruments used to detect and resolve systems are: AO det — adaptive optics; astdet — detection via astrometric perturbation, companion often not detected directly; astorb — orbit from astrometric measurements; HSTACS — *Hubble Space Telescope's* Advanced Camera for Surveys; HSTFGS — *Hubble Space Telescope's* Fine Guidance Sensors; HSTNIC — *Hubble Space Telescope's* Near Infrared Camera and Multi-Object Spectrometer; HSTWPC — *Hubble Space Telescope's* Wide Field Planetary Camera 2; lkydet — detection via lucky imaging; lkyorb — orbit from lucky imaging measurements; radorb — orbit from radial velocity measurements; radvel — detection via radial velocity, but no SB type indicated; SB (1, 2, 2O, 3) — spectroscopic binary, either single-lined, double-lined, double-lined with an orbit, or triple-lined; spkdet — detection via speckle interferometry; spkorb — orbit from speckle interferometry measurements; visdet — detection via visual astrometry; visorb — orbit from visual astrometry measurements

References— (1) this work; (2) Allen & Reid (2008); (3) Al-Shukri et al. (1996); (4) Balega et al. (2007); (5) Balega et al. (2013); (6) Bartlett et al. (2017); (7) Benedict et al. (2000); (8) Benedict et al. (2001); (9) Benedict et al. (2016); (10) Bergfors et al. (2010); (11) Bessel (1990); (12) Bessell (1991); (13) Beuzit et al. (2004); (14) Biller et al. (2006); (15) Blake et al. (2008); (16) Bonfils et al. (2013); (17) Bonnefoy et al. (2009); (18) Bowler et al. (2015); (19) Burningham et al. (2009); (20) Caballero (2009); (21) Chanamé & Gould (2004); (22) Cortes-Contreras et al. (2014); (23) Cvetković et al. (2015); (24) Daemgen et al. (2007); (25) Dahn et al. (1988); (26) Davison et al. (2014); (27) Dawson & De Robertis (2005); (28) Delfosse et al. (1999a); (29) Delfosse et al. (1999b); (30) Díaz et al. (2007); (31) Dieterich et al. (2012); (32) Docobo et al. (2006); (33) Doyle & Butler (1990); (34) Duquennoy & Mayor (1988); (35) Femenía et al. (2011); (36) Forveille et al. (2005); (37) Freed et al. (2003); (38) Fu et al. (1997); (39) Gizis (1998); (40) Gizis et al. (2002); (41) Golimowski et al. (2004); (42) Harlow (1996); (43) Harrington et al. (1985); (44) Hartkopf et al. (2012); (45) Heintz (1985); (46) Heintz (1987); (47) Heintz (1990); (48) Heintz (1991); (49) Heintz (1992); (50) Heintz (1993); (51) Heintz (1994); (52) Henry et al. (1999); (53) Henry et al. (2006); (54) Henry et al. (2018); (55) Høg et al. (2000); (56) Horch et al. (2010); (57) Horch et al. (2011a); (58) Horch et al. (2012); (59) Horch et al. (2015b); (60) Ireland et al. (2008); (61) Janson et al. (2012); (62) Janson et al. (2014a); (63) Janson et al. (2014b); (64) Jao et al. (2003); (65) Jao et al. (2009); (66) Jao et al. (2011); (67) Jenkins et al. (2009); (68) Jódar et al. (2013); (69) Köhler et al. (2012); (70) Kürster et al. (2009); (71) Lampens et al. (2007); (72) Law et al. (2006); (73) Law et al. (2008); (74) Leinert et al. (1994); (75) Lèpine et al. (2009); (76) Lindegren et al. (1997); (77) Luyten (1979a); (78) Makarov et al. (2008); (79) Malo et al. (2014); (80) Martín et al. (2000); (81) Martinache et al. (2007); (82) Martinache et al. (2009); (83) Mason et al. (2009); (84) Mason et al. (2018); (85) Mazeh et al. (2001); (86) McAlister et al. (1987); (87) McCarthy (1986); (88) Montagnier et al. (2006); (89) Nidever et al. (2002); (90) Pravdo et al. (2004); (91) Pravdo et al. (2006); (92) Reid et al. (2001); (93) Reid et al. (2002); (94) Reiners & Basri (2010); (95) Reiners et al. (2012); (96) Riddle et al. (1971); (97) Riedel et al. (2010); (98) Riedel et al. (2014); (99) Riedel et al. (2018); (100) Salim & Gould (2003); (101) Schneider et al. (2011); (102) Scholz (2010); (103) Ségransan et al. (2000); (104) Shkolnik et al. (2010); (105) Shkolnik et al. (2012); (106) Siegler et al. (2005); (107) Skrutskie et al. (2006); (108) Tokovinin et al. (2010); (109) Tokovinin & Lépine (2012); (110) van Biesbroeck (1974); (111) van Dessel & Sinachopoulos (1993); (112) Wahhaj et al. (2011); (113) Ward-Duong et al. (2015); (114) Weis (1991b); (115) Weis (1993); (116) Weis (1996); (117) Winters et al. (2011); (118) Winters et al. (2017); (119) Winters et al. (2018); (120) Woitas et al. (2003); (121) Zechmeister et al. (2009).

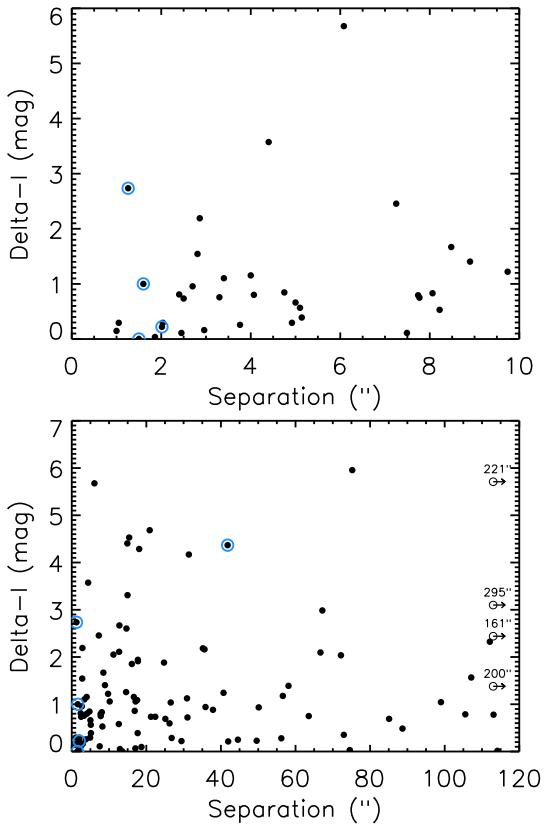

Figure 8. Solid points at ΔI vs. rho are plotted for companions detected during the Blinking and CCD Imaging Surveys to show the observational limits. The top plot is a zoom-in of the bottom. New companions discovered during our searches are encircled in blue. Open circles with arrows on the right represent companions that lie outside the range of the plot. From top to bottom, the companions are GJ 644E with ΔI = 5.71 and $\rho = 221''$, GJ 49B with $\Delta I = 3.10$ and $\rho = 295''$, G 192-011B with $\Delta I = 2.44$ and $\rho = 161''$ and, L 977-016B with $\Delta I = 1.38$ and $\rho = 200''$.

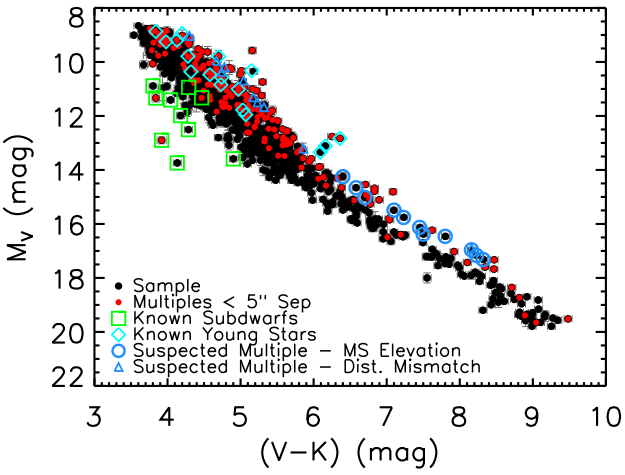

Figure 9. Observational HR Diagram for 1120 M dwarf primaries, with M_V plotted versus $(V-K)$ color. All stars are plotted with black points. Overplotted are known close multiples with separations less than $5''$ having blended photometry (red points), known subdwarfs (open green squares), and known young objects (open cyan diamonds). Error bars are shown in gray, and are smaller than the points, in most cases. The K magnitude errors for four objects with uncertain values (GJ0408, GJ0508.2, LHS3472, and LP876-026AB) have been omitted for clarity. As expected, known multiples with merged photometry are often elevated above the middle of the distribution. The 11 stars suspected to be new unresolved multiples due to their elevated positions relative to the main sequence are indicated with open blue circles. The ten stars suspected to be new unresolved multiples due to their distance mismatches from Figure 10 are indicated with open blue triangles. There are two objects that meet the criteria for both methods of identifying potential unresolved multiples. Note that the candidate multiples detected by main sequence elevation are mostly mid-to-late type M dwarfs, while the suspected multiples identified by the distance mismatch technique are primarily early-type M dwarfs.

boring unresolved stellar companions for nearly the entire sample. Various subsets of the sample were also probed using long-term astrometric data for stars observed during the RECONS astrometry program, as well as via data reduction flags indicating astrometric signatures of unseen companions for stars observed by *Hipparcos*. Listed in Table 6 are statistics for each companion search method. Note that the number of detections includes confirmations of previously reported multiples in the literature.

4.3.1. *Overluminosity via Photometry: Elevation Above the Main Sequence*

Accurate parallaxes and V and K magnitudes for stars in the sample allow the plotting of the observational HR Diagram shown in Figure 9, where M_V and the $(V-K)$ color are used as proxies for luminosity and temperature, respectively. Unresolved companions that contribute significant flux to the systems cause targets to be overluminous, placing them above the main sequence. Known multiples with separations $< 5''$ [12] are evident as points clearly elevated above the presumed single stars on the main sequence, and merge with a few young objects. Subdwarfs are located below and to the left of the

[12] This $5''$ separation appears to be the boundary where photometry for multiple systems from the literature — specifically from Bessell and Weis — becomes blended. For photometry available from the SAAO group (e.g., Kilkenny, Koen), the separation is $\sim 10''$ because they use large apertures when calculating photometric values.

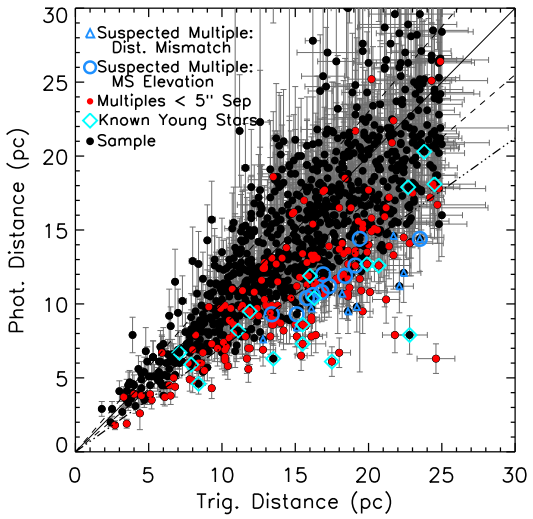

Figure 10. A comparison of distance estimates from $VRIJHK$ photometry vs. distances using π_{trig} for 1081 of the M dwarf primaries in the sample. The 31 stars with photometric distances > 30 pc are not included in this plot, nor are the eight primaries for which VRI are unavailable. Errors on the distances are noted in gray. The diagonal solid line represents 1:1 correspondence in distances, while the dashed lines indicate the 15% uncertainties associated with the CCD distance estimates from Henry et al. (2004). The dash-dot line traces the location where the trigonometric distance exceeds the photometric estimate by a factor of $\sqrt{2}$, corresponding to an equal-luminosity pair of stars. Known unresolved multiples with blended photometry are indicated with red points. The 11 candidate unresolved multiples from the HR Diagram in Figure 9 are enclosed with open blue circles. The ten new candidates that may be unresolved multiples from this plot are enclosed with open blue triangles. We note that one object — 2MA 1507-2000 — meets the criteria for both methods of identifying potential unresolved multiples.

singles, as they are old, metal-poor, and underluminous at a given color. Known young stars and subdwarfs are listed in Tables 13 and 14, along with their identifying characteristics. Eleven candidate multiples lying among the sequence of known multiples have been identified by eye via this HR Diagram. These candidates are listed in Table 12 and are marked in Figures 9 and 10. Note that these candiates are primarily mid-to-late M dwarfs.

4.3.2. *Overluminosity via Photometry: Trigonometric & CCD Distance Mismatches*

Because both VRI and 2MASS JHK photometry are now available for nearly the entire sample, photometric distances based on CCD photometry (*ccddist*) were estimated and compared to the accurate trigonometric distances (*trigdist*) available from the parallaxes. Although similar in spirit to the HR Diagram test discussed above that uses V and K photometry, all of the $VRIJHK$ photometry is used for each star to estimate the *ccddist* via the technique described in Henry et al. (2004), thereby leveraging additional information. As shown in Figure 10, suspected multiples that would otherwise have been missed due to the inner separation limit (2″) of our main imaging survey can be identified due to mismatches in the two distances. For example, an unresolved equal magnitude multiple would have an estimated *ccddist* closer by a factor of $\sqrt{2}$ compared to its measured *trigdist*.

With this method, 50 candidate multiples were revealed with *ccddists* that were $\sqrt{2}$ or more times closer than their *trigdists*. Of these, 40 were already known to have at least one close companion (36 stars), or to be young (four stars), verifying the technique. The remaining ten are new candidates, and are listed in Table 12.

4.3.3. *RECONS Perturbations*

A total of 324 red dwarfs in the sample have parallax measurements by RECONS, with the astrometric coverage spanning 2–16 years. This number is slightly higher than the 308 parallaxes listed in Table 2, due to updated and more accurate RECONS parallax measurements that improved upon YPC parallaxes with high errors. The presence of a companion with a mass and/or luminosity different from the primary causes a perturbation in the photocenter of the system that is evident in the astrometric residuals after solving for the proper motion and parallax. This is the case for 39 of the observed systems, which, although sometimes still unseen, are listed as confirmed companions in Table 11, where references are given. This is the only technique used in this companion search that may have revealed brown dwarf companions, although in several cases the companion has not yet been resolved, so it remains uncertain whether the companion is a red or brown dwarf. When uncertain, we assume that the companion is a red dwarf.

4.3.4. *Hipparcos Reduction Flags*

All 460 stars in the sample with *Hipparcos* parallaxes were searched for entries in the Double and Multiple Systems Annex (DMSA) (Lindegren et al. 1997) of the original *Hipparcos* Catalog to reveal any evidence of a companion. Of these 460 stars, 229 have a parallax measured only by *Hipparcos*, while 231 also have a parallax measurement from another source. Various flags exist in the DMSA that confirm or infer the presence of a companion: C — component solutions where both components are resolved and have individual parallaxes; G — acceleration solutions, i.e., due to variable proper motions,

Table 12. Suspected Multiple Systems

Name	# Stars	RA (hh:mm:ss)	DEC (dd:mm:ss)	Flag	Reference
GJ1006A	3?	00 16 14.6	+19 51 37	dist	1
HIP006365	2?	01 21 45.3	−46 42 51	X	3
LHS1288	2?	01 42 55.7	−42 12 12	X	3
GJ0091	2?	02 13 53.6	−32 02 28	X	3
GJ0143.3	2?	03 31 47.1	+14 19 17	X	3
BD-21-01074A	4?	05 06 49.9	−21 35 08	dist	1
GJ0192	2?	05 12 42.2	+19 39 56	X	3
GJ0207.1	2?	05 33 44.8	+01 56 43	possSB	4
SCR0631-8811	2?	06 31 31.7	−88 11 38	elev	1
LP381-004	2?	06 36 18.2	−40 00 23	G	3
SCR0702-6102	2?	07 02 49.7	−61 02 52	elev,pb?	1,1
LP423-031	2?	07 52 24.0	+16 12 15	elev	1
SCR0757-7114	2?	07 57 32.5	−71 14 53	dist	1
GJ1105	2?	07 58 12.7	+41 18 13	X	3
LHS2029	2?	08 37 07.9	+15 07 45	X	3
LHS0259	2?	09 00 52.1	+48 25 25	elev	1
GJ0341	2?	09 21 37.6	−60 16 55	possSB	4
GJ0367	2?	09 44 29.8	−45 46 35	X	3
GJ0369	2?	09 51 09.6	−12 19 47	X	3
GJ0373	2?	09 56 08.6	+62 47 18	possSB	4
GJ0377	2?	10 01 10.7	−30 23 24	dist	1
GJ1136A	3?	10 41 51.8	−36 38 00	X,possSB	3,4
GJ0402	2?	10 50 52.0	+06 48 29	X	3
LHS2520	2?	12 10 05.0	−15 04 16	dist	1
GJ0465	2?	12 24 52.0	−18 14 32	pb?	2
DEN1250-2121	2?	12 50 52.2	−21 21 09	elev	1
GJ0507.1	2?	13 19 40.1	+33 20 47	X	3
GJ0540	2?	14 08 12.9	+80 35 50	X	3
2MA1507-2000	2?	15 07 27.7	−20 00 43	dist,elev	1
G202-016	2?	15 49 36.2	+51 02 57	G	3
LHS3129A	3?	15 53 08.7	+34 44 39	dist	1
GJ0620	2?	16 23 07.6	−24 42 35	G	3
GJ1203	2?	16 32 45.1	+12 36 45	X	3
LP069-457	2?	16 40 14.7	+67 36 32	elev	1
LTT14949	2?	16 40 48.9	+36 19 00	X	3
HIP083405	2?	17 02 49.5	−06 04 06	X	3
LP044-162	2?	17 57 15.0	+70 42 01	elev	1
LP334-011	2?	18 09 40.7	+31 52 12	X	3
SCR1826-6542	2?	18 26 46.8	−65 42 38	elev	1
LP044-334	2?	18 40 02.0	+72 40 54	elev	1
GJ0723	2?	18 40 17.8	−10 27 54	X	3
HIP092451	2?	18 50 26.6	−62 03 03	possSB	4
LHS3445A	3?	19 14 39.1	+19 19 03	dist	1
GJ0756	2?	19 21 51.4	+28 39 58	X	3
LP870-065	2?	20 04 30.7	−23 42 01	dist	1
GJ1250	2?	20 08 17.9	+33 18 13	dist	1
LEHPM2-0783	2?	20 19 49.8	−58 16 40	elev	1
GJ0791	2?	20 27 41.6	−27 44 51	X	3
LHS3564	2?	20 34 43.0	+03 20 51	X	3
GJ0811.1	2?	20 56 46.6	−10 26 54	X	3
L117-123	2?	21 20 09.8	−67 39 05	X	3
HIP106803	2?	21 37 55.6	−63 42 42	X	3
LHS3748	2?	22 03 27.1	−50 38 38	X	3
G214-014	2?	22 11 16.9	+41 00 54	X	3
GJ0899	2?	23 34 03.3	+00 10 46	X	3
GJ0912	2?	23 55 39.7	−06 08 33	X	3

References—(1) this work; (2) Heintz (1986); (3) Lindegren et al. (1997); (4) Reiners et al. (2012).

NOTE—Flag Description: **dist** means that the *ccddist* is at least $\sqrt{2}$ times closer than the *trigdist* due to the object's overluminosity; **elev** means that the object is elevated above the main sequence in the HR Diagram in Figure 9 due to overluminosity; **possSB** means that the object has been noted as a possible spectroscopic binary by Reiners et al. (2012); **pb?** indicates that a possible perturbation was noted. The the single letters are *Hipparcos* reduction flags as follows: *G* is an acceleration solution where a component might be causing a variation in the proper motion; *V* is for Variability-Induced Movers, where one component in an unresolved binary could be causing the photocenter of the system to be perturbed; *X* is for a stochastic solution, where no reliable astrometric parameters could be determined, and which may indicate an astrometric binary.

which could be caused by an unseen companion; O — orbits from astrometric binaries; V — Variability-Induced Movers (VIMs), where the variability of an unresolved companion causes the photocenter of the system to move or be perturbed; X — stochastic solutions, for which no astrometric parameters could be determined and which may indicate that the star is actually a short-period astrometric binary.

Most of the AFGK systems observed by *Hipparcos* that have flags in the DMSA have been further examined or re-analyzed by Pourbaix et al. (2003, 2004), Platais et al. (2003), Jancart et al. (2005), Frankowski et al. (2007), Horch et al. (2002, 2011a,b, 2015a, 2017); however, few of the M dwarf systems have been investigated to date. Stars with C and O flags were often previously known to be binary, are considered to be confirmed multiples, and are included in Table 11. We found that G, V, or X flags existed for 31 systems in the survey — these suspected multiples are listed in Table 12.

4.4. *Literature Search*

Finally, a literature search was carried out by reviewing all 1120 primaries in *SIMBAD* and using the available bibliography tool to search for papers reporting additional companions. While *SIMBAD* is sometimes incomplete, most publications reporting companions are included. Papers that were scrutinized in detail include those reporting high resolution spectroscopic studies (typically radial velocity planet searches or $v\sin i$ results that might report spectroscopic binaries), parallax papers that might report perturbations, high resolution imaging results, speckle interferometry papers, and other companion search papers. A long list of references for multiple systems found via the literature search is included in Table 11.

In addition, the Washington Double Star Catalogue (WDS), maintained by Brian Mason[13], was used extensively to find publications with information on multiple systems. Regarding the WDS, we note that: (1) not all reported companions are true physical members of the system with which they are listed, and (2) only resolved companions (i.e., no SBs) are included in the catalog. Thus, care had to be taken when determining the true number of companions in a system. Information pertaining to a star in the WDS was usually only accessed after it was already known that the system was multiple and how many components were present in the system, so this was not really troublesome. However,

[13] The primary copy is kept at USNO and a back-up copy is housed at Georgia State University.

the WDS sometimes had references to multiplicity publications that *SIMBAD* had not listed. Thus, the WDS proved valuable in identifying references and the separations, magnitude differences, and other information included in Table 11.

Finally, an additional six stars were reported as suspected binaries in the literature: GJ 207.1, GJ 341, GJ 373, GJ 1136A and HIP 92451 were noted by Reiners et al. (2012) as possible spectroscopic binaries, and GJ 465 was identified by Heintz (1986) as a possible astrometric binary. These are listed in Table 12. In a few cases, a star may have more than one indication that it is an unresolved multiple.

5. RESULTS

In this section we report the multiplicity and companion rates for the 1120 M dwarfs surveyed, before any corrections are applied. The *Multiplicity Rate* (MR) is the percentage of all systems that are multiple, regardless of whether the system is double, triple or higher order. For example, discovering that a member of a binary system has additional close companion makes the system a triple, but would not affect the multiplicity rate. The *Companion Rate* (CR) is the average number of companions per primary in the sample, so higher order multiples *do* affect this rate, as they add a companion to the statistics. The equations describing these percentages are given below, where N_S is the number of Singles, N_D is the number of Doubles, N_T is the number of Triples, N_{Qd} is the number of Quadruples, and N_{Qn} is the number of Quintuples, the highest order multiples so far known among M dwarf primaries within 25 pc. The denominator in both cases is 1120.

$$MR = 100 * \frac{N_D + N_T + N_{Qd} + N_{Qn}}{N_S + N_D + N_T + N_{Qd} + N_{Qn}} \quad (1)$$

$$CR = 100 * \frac{N_D + 2N_T + 3N_{Qd} + 4N_{Qn}}{N_S + N_D + N_T + N_{Qd} + N_{Qn}} \quad (2)$$

We analyze all companions in relation to the primary of the system, even if they are members of sub-binaries or -triples.

5.1. *Multiplicity and Companion Rates for Confirmed Companions*

Among the 1120 M dwarfs searched, there are 265 multiple systems with 312 new and confirmed *stellar* companions to their primaries, resulting in an initial uncorrected multiplicity rate of MR = 23.7±1.3% and an uncorrected stellar companion rate of CR = 27.9±1.3%. The ratios of singles:doubles:triples:higher-order systems is 856:223:39:3, corresponding to 76.4:19.9:3.5:0.3%. For comparison, Raghavan et al. (2010) found 56:33:8:3% for singles:doubles:triples:higher-order systems for companions (including brown dwarfs) in a sample of 454 solar-type stars. If we include the known brown dwarf companions to M dwarfs, the ratios change only slightly, to 844:230:43:2:2, corresponding to 75.3:20.5:3.8:0.3%. **Thus, three-quarters of M dwarfs are single, compared to only half of solar-type stars.**

Information for all multiple systems (including brown dwarf components) is presented in Table 11, with *n-1* lines for each system, where n is the total number of components in the system. For example, a quadruple system will have three lines of information that describe the system. The name is followed by the number of components in the system and the configuration map of the components detailed in that line of the Table. If the line of data pertains to higher order systems containing component configurations for sub-systems (e.g., 'BC' of a triple system), the number of components noted will be '0', as the full membership of the system will already have been noted in the line of data containing the 'A' component. These data are followed by epoch J2000.0 coordinates, the angular separation (ρ) in arcseconds, the position angle (θ) in degrees measured East of North, the year of the measurement, the code for the technique used to identify the component, and the reference. We assign a separation of $<1''$ for all astrometric and spectroscopic binaries (unless more information is available) and/or to indicate that a companion has been detected, but not yet resolved. We note that where orbit determinations from the literature are reported, the semimajor axis, a, is listed instead of ρ. If a was not reported in the reference given, it was calculated from the period and the estimated masses of the components in question via Kepler's Third Law.

The final three columns give a magnitude difference (Δmag) between the components indicated by the configuration map, the filter used to measure this Δmag, and the reference for this measurement. Photometry from photographic plates is denoted by 'V*'. In many cases, there are multiple separation and Δmag measurements available in the literature from different groups using different techniques. An exhaustive list of these results is beyond the scope of this work; instead, a single recent result for each system is listed. In a few cases, the position angles and/or Δmag measurements are not available.

Figure 11 illustrates the projected separations of the 292 confirmed, 20 new, and 56 suspected stellar companions from their primaries. A Gaussian curve has been

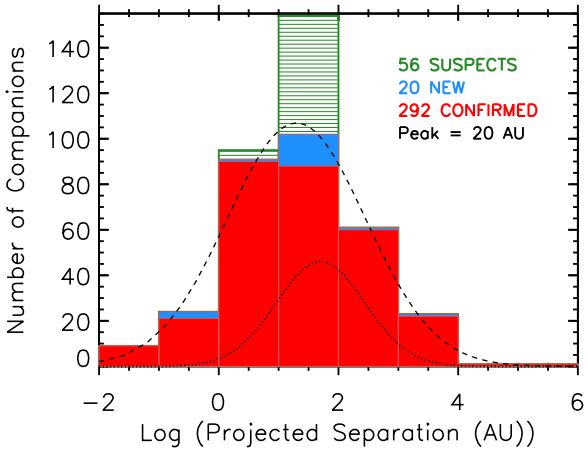

Figure 11. A histogram of the distribution of the projected separations of all stellar companions from their red dwarf primaries, in log form for clarity. The 292 confirmed (in red), 20 new (in blue), and 54 suspected companions (in green) are indicated. The dashed curve is a Gaussian that has been fit to the distribution of confirmed and new (but not suspected) companions and has a peak at 20 AU, with $\sigma_{loga} = 1.16$. For comparison, the dotted line indicates the fit for solar-type stars from Raghavan et al. (2010), which peaks at 51 AU, with $\sigma_{logP} = 2.28$ yr.

fit to the distribution of confirmed and new (but not suspected) companions as a function of log-separation, providing a reasonable fit to the distribution as known in the current dataset. Exoploration of fitting a skewed Gaussian curve to the data resulted in a skew value very close to zero, with a peak at 20 AU. Therefore, we justify our use of a normal Gaussian curve in this analysis. In an even larger sample that has been completely searched for companions at small separations, a different distribution may prove to be more appropriate.

The peak in the separation distribution falls at 20 AU, with a broad spread indicating that most stellar companions to M dwarfs are found at separations on the scale of our Solar System, i.e., 1–100 AU. This distribution peaks at larger projected separations than the one presented in Janson et al. (2014a) for mid-type M dwarfs (6 AU, their Figure 3). However, their search was for companions at angular separations 0.″08–6″ from their primaries at inferred distances within 52 pc (corresponding to 4–312 AU), whereas our study searched for companions at angular separations out to 300″, corresponding to separations as large as 7500 AU at the survey horizon of 25 pc. In addition, their results are based on a sample containing 91 pairs in 85 multiples (from 79 binaries and six triples), compared to our 312 pairs in 265 multiples. Similarly, the distribution peak that we find is also at much larger separations than the 5.3 AU peak reported for stars $0.1 \lesssim M/M_{\odot} \lesssim 0.5$ by Duchêne & Kraus (2013), i.e. M dwarfs. Comparing our sample to solar-type stars, the peak for M dwarfs at 20 AU (dashed line) is roughly one-half the distance for the peak at 51 AU for the 259 companions found to 454 stars (dotted line) by Raghavan et al. (2010). In summary, **stellar companions to M dwarfs are most often found at separations similar to that of our Solar System, and at roughly half the distance of stellar companions to more massive, solar-type, stars.**

The distribution shown in Figure 11 represents the projected separations observed, but two possible shifts in the distribution for these confirmed companions should be noted. Incorporating the correction of a factor of 1.26 from Fischer & Marcy (1992) for those systems for which no orbital information is known (all but 33 of the systems presented here), would shift the distribution to larger separations. In the opposite sense, we adopted projected separations of 1″ for unresolved systems, which is the case for 33 of the confirmed and new companions, plus all of the 56 suspected systems; these generally should be considered upper limits. Consequently, the distribution shown in Figure 11 will shift leftward to smaller separations once all known close companions have orbital semimajor axes determined.

5.2. *Suspected Companions*

Forty-nine singles suspected to be doubles were revealed during this survey, three of which (GJ 912, GJ 1250, and SCR 1826-6542) have so far been confirmed with continuing follow-up observations. An additional five doubles are suspected to be triples, yielding a current total of 54 suspected additional companions (only one companion per system in all cases) listed in Table 12, but *not* included in Table 11.[14] Systems in Table 12 are listed with the suspected number of components followed by a question mark to indicate the system's suspect status, followed by J2000.0 coordinates, a flag code for the reason a system is included as having a candidate companion, and the reference. Notes to the table give detailed descriptions of the flags. Among the 56 suspected companions, 31 are from the *Hipparcos* DMSA, in which they are assigned G, V, or X flags. A number of primaries that were suspected to be multiple due to either an underestimated *ccddist* or an elevated position on the HR diagram were found through the literature search to have already been resolved by others and

[14] For consistency, companions to GJ 912, GJ 1250, and SCR 1826-6542 are included in Table 12 and in the 'Suspects' portion of the histogram in Figure 11.

have been incorporated into Table 11 and included in the analysis as confirmed companions. There remain 21 systems in Table 12 with *ccddist* values that do not match their trigonometric parallax distances and/or that are noticeably elevated above the main sequence that have not yet been confirmed. A few more systems had other combinations of indicators that they were multiple, e.g., an object with a perturbation might also have a distance mismatch. We reiterate that none of these *suspected* companions have been included in any of the analyses of the previous section or that follow; only *confirmed* companions have been used.

5.3. *Substellar Companions*

Because this study focuses on the *stellar* companions of M dwarfs, it was important to determine which companions were stellar and which were *substellar*. Dieterich et al. (2014) found that the boundary between stars and brown dwarfs is near the L2.0V spectral type; efforts are underway to determine to what mass this spectral type corresponds. As mentioned in §2, $M_V = 20.0$ and $(V-K) = 9.5$ were used as cutoffs for the faintest and reddest (and correspondingly least massive) M dwarfs. Analysis of the main sequence in the HR diagram created from the RECONS list of stars and brown dwarfs within 25 pc indicates that $M_V = 21.5$ and $(V-K) = 10.3$ correspond to spectral type L2.0V, and therefore the end of the stellar main sequence. Thus, for this large statistical study, we consider objects fainter or redder than these limits to be substellar brown dwarfs.

Via the literature search, 17 brown dwarf companions to 15 M dwarf primaries were identified. These are noted in Table 4 with a 'BD' for the component in the object column (column 2). Although no comprehensive searches have been done for brown dwarfs as companions to the 1120 M dwarfs targeted here (including ours), we note that as presently known, the rate of M dwarf primaries with known brown dwarf companions is only 1.3 ± 0.3%. This is a factor of twenty less than the stellar multiplicity rate, considering the stellar and brown dwarf companions detected to date. While more brown dwarf companions will undoubtedly be found in the future, they are much rarer than stellar companions. We note that astrometric detection via a perturbation is the only technique used in this survey that was sensitive to brown dwarf companions, and only a few stars (GJ 1215, SCR 1845-6357) have so far been found to be orbited by brown dwarfs via perturbations in data from our astrometric survey at the CTIO/SMARTS 0.9m.

We do not include any brown dwarf companions in the analysis that follows. Dynamical masses have not yet been measured for most of these objects. Furthermore, a mass-luminosity relation does not yet exist which would permit the determination of masses for these objects, a key component to our analysis. We do not address planetary companions in this work.

6. ADJUSTMENT TO THE MULTIPLICITY RATE AT SMALL SEPARATIONS

Because this survey was not uniformly sensitive to systems with companions at $\rho \leq 2''$, a correction should be made in order to determine a final multiplicity rate. The sample of M dwarfs within 10 pc appears to be at least 90% complete based on decades of RECONS work. Thus, this volume-limited 10 pc sample provides a reasonably complete set of stars that can provide insight to the stellar companion rate at small separations, if effectively all of the primaries have been targeted by some kind of high resolution technique. An adjustment based on the stellar multiplicity rate of those objects for the closest companions can be determined and applied to the sample of 1120 M dwarfs in the full survey outlined here.

A literature search for spectroscopic and high resolution imaging studies targeting M dwarfs within 10 pc was performed to determine the companion population at small separations. These two techniques cover most of the separation phase space for stellar companions at separations $\rho < 2''$. It was found that all but two systems either already had a close companion at $\rho < 2''$, or had been observed with high resolution techniques, e.g., spectroscopy, *HST* imaging, speckle interferometry, lucky imaging, or long-term astrometry. Because 186 of the 188 M dwarfs within 10 pc have been searched, we infer that we can use the 10 pc sample to correct for unresolved companions with $\rho < 2''$ at distances 10–25 pc.

Figure 12 presents a graph of the running stellar multiplicity at different angular separations as a function of distance for the sample of M dwarfs found within 25 pc. For the 10 M dwarfs with substellar companions, the system was considered single for the purpose of the stellar multiplicity calculation. For the five triple systems containing substellar companions, the three that had two substellar companions were considered single, while the two systems that had both an M dwarf and a substellar companion were considered multiple. For higher order multiple systems with more than one companion, the smallest separation between the primary and a companion was chosen to mitigate the likely incompleteness at small ρ.

The striking feature of Figure 12 is that most stellar companions to red dwarfs are found at separations less than $2''$. Thus, it is not surprising that the two

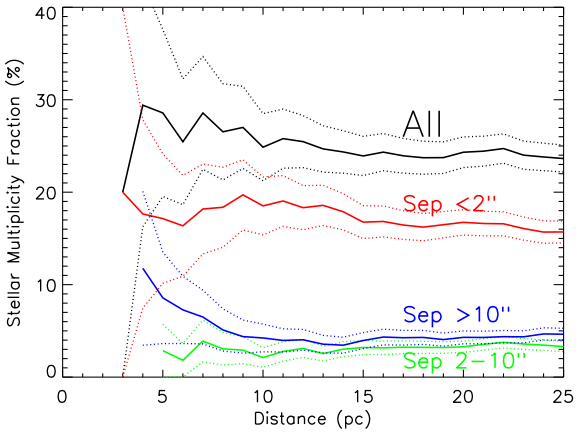

Figure 12. The cumulative multiplicity rate at different angular separations for the 265 multiples among 1120 M dwarf systems, binned by one parsec and subdivided into separations of ρ less than 2″, $\rho = 2 - 10''$, and ρ greater than 10″. The two rates for companions with separations greater than 2″ remain fairly constant from 10 to 25 pc, while the rate for separations smaller than 2″ decreases slightly from ∼10 to 25 pc, and particularly from 13–25 pc, indicating that a correction is warranted. Neither suspected nor substellar companions are included in this graph, and for multiple systems with more than one companion, the companion with the smallest separation from its primary was used. The dotted lines indicate the binomial errors on each line. The large scatter and errors on the curves at distances less than 10 pc are due to small samples of stars.

main campaigns for detecting companions undertaken here yielded few new objects, yet those searches needed to be done systematically. It is evident that the two sets of companions at separations greater than 2″ are effectively constant from 10 to 25 pc, indicating that there are not significant numbers of overlooked companions at large separations from their primaries. The multiplicity rates for companions with angular separations 2–10″ and > 10″ are 3.5% and 4.6%, respectively, indicating that 8.1% of the nearest M dwarfs have companions beyond 2″. In contrast, the curve for companions with separations smaller than 2″ decreases from 10 pc to 25 pc, implying that more close companions remain to be found from 10–25 pc. Many of these are presumably the candidates discussed in §5.2 and listed in Table 12.[15] By comparing the multiplicity rate for $\rho <$ 2″ at 10 pc (35/188 = 18.6±2.8%) to the rate at 25 pc (176/1120 = 15.7±1.1%), we find a correction of an additional 2.9±0.5% companions that can be appropriately applied to stars from 10–25 pc. This corresponds to 27 companions among the 933 stars in this shell, bringing the total number of M dwarfs within 25 pc to 265 + 27 = 292 for 1120 primaries. Thus, the corrected multiplicity rate for the entire sample is 26.1±1.4%.

[15] We note that four of the stars suspected to be multiple are located within 10 pc. All four have been observed with both high resolution spectroscopy and imaging, with no companions detected. If any are found to have a companion, the correction will change, but that appears unlikely to happen.

7. MASSES FOR RED DWARFS IN THE SAMPLE

In order to perform any quantitative analysis of the multiplicity results related to stellar mass, a conversion from M_V to mass using a mass-luminosity relation (MLR) was necessary for each primary and companion in the sample. For single M dwarfs or wide binaries with separate V photometry, this is straightforward. For multiples with separations less than ∼4″, system photometry was deblended at V using Point Spread Function (PSF) fits. For multiples too close for PSF photometry, estimates of the Δmags were made based on the information available in the literature.

7.1. *Deblending Photometry*

For systems with companions at separations too small (typically 1–4″) to perform effective aperture correction photometry, PSF photometry was performed on frames acquired in Arizona and Chile during the imaging program in order to measure ΔV for each system. First, the contribution from the sky background was calculated from a 'blank' part of the image. The region around the close pair being analyzed was then cropped, as we were only interested in the relevant pair, and the background subtracted. A Moffat curve was fit to the PSF of the primary, the flux determined from the fit, and then the primary was subtracted from the image, with care taken to minimize the residual counts from the primary. Gaussian and Lorentzian curves were also tested, but it was found that Moffat curves provided the best fits to PSFs from all of the 1m-class telescopes used in this program. A Moffat curve was then fit to the secondary component's PSF and the flux calculated from the fit. The ratio of the fluxes of the primary and secondary yielded the ΔV, which, when combined with the V photometry, provided the individual V magnitudes needed to estimate masses for each component in a multiple.

For triples having where all three components were closer than 4″, the pair with the widest separation was deblended first using the appropriate ΔV to calculate the deblended V magnitude for the single and the resulting pair. Then the ΔV relevant to the remaining pair was used to calculate individual V magnitudes for the components of the closest pair.

For the many close multiples with Δmags reported in the literature that were not in the V-band, the rela-

tions reported in Riedel et al. (2014) were used to convert ΔR_{KC}, ΔI_{KC}, $\Delta r'$, $\Delta i'$, or 2MASS ΔJ, ΔH, or ΔK filters to ΔV_J. Magnitude differences from the *Hipparcos* H_p and *Tycho-2* V_T filters were considered to be equivalent to V_J, as were any visual Δmags reported in the literature, e.g., those from any binary papers before ∼1995 that used photographic plates. For results using the Differential Speckle Survey Instrument (DSSI) (Horch et al. 2009) reported in Horch et al. (2011a, 2012, 2015b), Δ562 was adopted to be ΔV and Δ692 was adopted to be ΔR. Horch et al. (2009) state that the 562 and 692 nm DSSI filters' central wavelengths are close to those of the V and R of the Johnson $UBVRI$ system. For observations from the RIT-Yale Tip-tilt Speckle Imager (RYTSI) (Meyer et al. 2006) reported in Horch et al. (2010, 2012), Δ550 measurements were adopted as ΔV, Δ698 were adopted as ΔR, and Δ754 nm measurements were adopted as ΔI. The Δ814 measurements reported in Reid et al. (2001) were assumed to be ΔI. For *HST* data, the $F110W$ and $F222M$ filters were considered similar enough to J and K to not require conversions in Δmags.

We note that for pairs with ΔV values larger than 3.0, the mass of the primary was calculated using the observed V magnitude as if it were single, as a companion with that ΔV contributes negligible flux (∼6% or less) to the system. Although the ΔVs are often not well-defined at differences this large, the ΔV was simply added to the V magnitude of the primary and the mass estimated for the companion using that V.

Systems with unknown magnitude differences between the components (i.e., typically those with separations $<1''$) required estimates of the Δmag, which were made as follows: (1) SB2s were assigned $\Delta\text{mag} = 0$, (2) SB1s were assigned $\Delta\text{mag} = 1$, and (3) unresolved astrometric detections were assigned $\Delta\text{mag} = 2$. These estimates were all done for the filter in which the observations were done or reported; e.g., an object with a perturbation that was being observed in the $I-$band by the RECONS group at the CTIO/SMARTS 0.9m was noted as having $\Delta I = 2$, which was then converted to ΔV.

The ΔV and deblended V magnitudes for the individual components of multiple systems are given in Table 4, with the estimate in italics if any of the aforementioned assumptions were made. This is the case for roughly half of the pairs. We note that while some of the current ΔV estimates are imperfect, a current project using speckle imaging to measure magnitude differences directly is in progress.

7.2. *Estimating Masses*

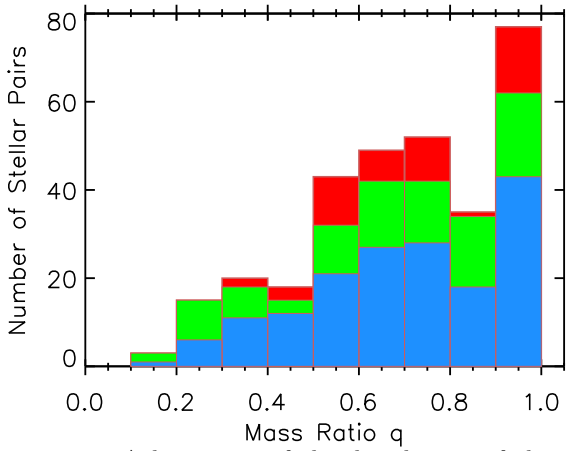

Figure 13. A histogram of the distribution of the mass ratios (M_2/M_1, M_3/M_1, etc.) of the 312 stellar pairs in the sample. In blue are plotted pairs for which no conversion or assumption to ΔV was made, green indicates a conversion to ΔV from another filter, and red indicates that an assumption was made regarding the Δmag. The distribution is likely incomplete at mass ratios less than 0.5 and uniform from 0.5 to equal mass ratios of 1.0, as the red shaded portions of the histogram will likely shift left-ward in the future. We note that no corrections due to 'missing' multiple systems have been incorporated into this distribution, nor are brown dwarf companions included.

A robust mass-luminosity relation (MLR) for red dwarfs has recently been provided by Benedict et al. (2016), using extensive sets of *HST-FGS* and radial velocity data. We use their results on 47 stars with masses 0.07–0.62 $M_\odot$ (average errors of 0.005 $M_\odot$) to estimate masses for the red dwarfs in the survey outlined here. Using their mass-M_V relation, which has a scatter of 0.017 $M_\odot$, the massive end of the M dwarf spectral sequence for which we have adopted $M_V = 8.8$ corresponds to 0.63 $M_\odot$. The least massive M dwarf with $M_V = 20.0$ results in a mass of 0.075 $M_\odot$, consistent with the lowest mass M dwarf in Benedict et al. (2016), GJ1245C with mass = 0.076 ± 0.001 $M_\odot$.

Twenty-nine of the objects in our survey had masses presented in Benedict et al. (2016) that were used to define the MLR. This provides an opportunity to assess the accuracy of the mass estimates assigned here. We find a mean absolute deviation between the measured masses and our estimates of 10.5%, differences that can be attributed to cosmic scatter, as discussed in Benedict et al. (2016). Mass estimates for all components are listed in Table 4.

7.3. *Mass Ratios*

With mass estimates for all the stars in multiple systems in-hand, we can evaluate the mass ratios of all

companions relative to their primaries. Figure 13 shows the distribution of the mass ratios ($q = M_{comp}/M_{pri}$) for the 312 pairs in the sample. All companions were analyzed in relation to the primary of the system. There are 223 binaries, as well as 39 triples that result in 78 pairs of objects, one quadruple system yielding three pairs, and the two quintuple systems yielding eight pairs. In the instances where Δmags reported in the literature for hierarchical systems was other than with respect to the 'A' component, these data were calculated by first deblending the pair in question, calculating individual magnitudes, estimating individual masses, and then calculating the mass ratios in relation to the primary.

As shown in Figure 13, most of the pairs in the sample have mass ratios larger than 0.5 with a distribution that may very well be flat from q = 0.5–1.0, particularly given that accurate determinations of the pairs represented in red in the histogram may shift the distribution left-ward somewhat. For $q < 0.5$, there are a few incompleteness effects. First, we have excluded from the analysis the 17 known brown dwarf companions, which affect mass ratio evaluations more for M dwarfs than for any other type of star. Second, we show in §8.1 that primaries with masses 0.075–0.30 $M_\odot$ likely have companions that have eluded detection. These missing companions might fill in various parts of the distribution, but only for $q > 0.25$ (0.075 $M_\odot$/0.30 $M_\odot$), where 0.25 is the smallest q value possible in that mass regime when considering only *stellar* companions.

In order to assess whether the trend from q = 0.5–1.0 is real or due to a bias in the way the ΔV values were calculated (as described above), the histogram has been color-coded in order to identify any trends: blue represents pairs with Δmag in V (167 pairs), green represents pairs for which a conversion from a Δmag other than ΔV was made (96 pairs), and red represents pairs for which an assumption had to be made about the Δmag between the two components, e.g., unresolved spectroscopic binaries and astrometric perturbations (49 pairs). We do not see any strong systematic trend that correlates with the assumptions or conversions that were used for the mass estimates.

8. DEPENDENCE OF M DWARF MULTIPLICITY ON VARIOUS CHARACTERISTICS

Exploring how the multiplicity of M dwarf systems depends on various characteristics provides hints about star formation processes. Because the target sample includes more than 1000 stars and more than 300 pairs, we can evaluate trends in multiplicity as functions of mass, separation, and tangential velocity, the latter of which can be used at some level as a proxy for age.

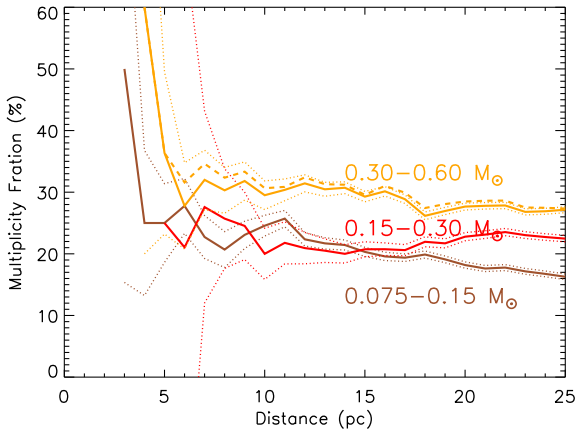

Figure 14. Cumulative stellar multiplicity rate by primary mass. Shown are the running multiplicity rates of the three mass subsets binned by one parsec, with the masses of the primaries calculated from deblended photometry: primary masses 0.30–0.60 $M_\odot$ represented by the orange line, with an uncorrected multiplicity rate of 27.8 ± 2.3%; primary masses 0.15–0.30 $M_\odot$ shown by the red line with an uncorrected multiplicity rate of 20.8 ± 2.6%; and primary masses 0.075–0.15 $M_\odot$ shown by the brown line, with an uncorrected multiplicity rate of 15.8 ± 2.6%. The dashed orange line indicates the addition of the 26 systems that have a primary mass larger than 0.60 $M_\odot$. The largest mass bin has a higher multiplicity rate than the two smaller mass bins. It appears likely that multiple systems are missing from the smallest mass bin at distances 18 to 25 pc, as the curve decreases at those distances. The dotted lines on each curve indicate the Poisson errors. The large scatter and errors on the curves at distances less than 10 pc are due to small number of statistics. Neither suspected nor substellar companions are included.

8.1. *M Dwarf Multiplicity as a Function of Mass*

It is known that the multiplicity rate decreases with the mass of the primary star for spectral types O through G (Duchêne & Kraus 2013), and one of the primary goals of our survey is to determine if that trend continues as a function of primary mass through the M dwarfs.

Figure 14 illustrates the multiplicity rate dependence for three mass regimes — 0.30–0.60 $M_\odot$, 0.15–0.30 $M_\odot$, and 0.075–0.15 $M_\odot$ — as a function of distance to the target stars. The sample is subdivided into mass bins that span different factors of two, and no corrections have been applied for undetected companions in any of the three subsamples. The dashed orange line shows the contribution of the 26 systems that have a primary mass larger than 0.60 $M_\odot$, of which eight are multiple. It is evident that the highest mass bin has the highest multiplicity rate at 15 pc (29.3 ± 3.4%), roughly 10% greater than for lower masses (20.7 ± 2.8% and 20.3 ± 3.6% for

the mid- and low-mass bins, respectively). These values are consistent with Figure 3 in Janson et al. (2012) and Figure 7 in Janson et al. (2014a), although their sample only extends to spectral type M6, so they do not address our lowest mass bin. It also appears that there are slight dropoffs in detected multiples for the highest and lowest mass bins from 15 to 25 pc, whereas the multiplicity rate for the medium-mass bin remains flat. The dropoff for the highest mass stars is only 2%, a shift that we deem insignificant. However, the dropoff for the lowest mass stars is 4% from 15 to 25 pc and in fact is 9% from 11 to 25 pc. This is likely because the lowest mass primaries are the most difficult to study, so some companions have yet to be detected. Nonetheless, the overall situation is clear: **high mass M dwarfs have more companions than low mass M dwarfs.**

With our large sample, it is also possible to evaluate the dependence of mass ratios in multiple systems on primary mass. Figure 15 presents the mass ratios (top row of three plots) and the log of the projected separations in AU (bottom row of three plots, discussed below) of the 312 stellar components as functions of primary mass. The axis scales were kept the same between each trio of plots in order to highlight the changes for various mass regimes.

It is evident that the number of multiples in each subset decreases with decreasing primary mass, as shown more explicitly in Figure 14. Of note is the wide range in the mass ratios for the most massive primaries, indicating that such stars tend to form with companions filling nearly the entire suite of possible masses. There is also a general shift to larger mass ratios with decreasing primary masses. This trend is somewhat expected because we have set a hard limit on companion masses by only including stellar companions, and there is a decreasing amount of mass phase space available as the primary's mass approaches this stellar/sub-stellar boundary; as noted in §5.3, brown dwarf companions have been excluded from the analysis. However, the percentage of M dwarfs in this sample with known brown dwarf companions is 1.3%, a rate too low to fill in the extreme mass ratios for the lowest mass primaries. We note that this rate is consistent with the number of solar-type stars with brown dwarf companions in the sample studied by Raghavan et al. (2010): 7/454 = 1.5%. Furthermore, as shown by Dieterich et al. (2012), there are not many brown dwarfs found around small stars. Thus, it appears that lower mass red dwarfs may only form and/or gravitationally retain companions when they are of comparable mass and at small separations. **We conclude that high mass M dwarfs have nearly every type of lower mass companion star, whereas low mass M dwarfs do not, and even when considering brown dwarfs as companions, this remains true.**

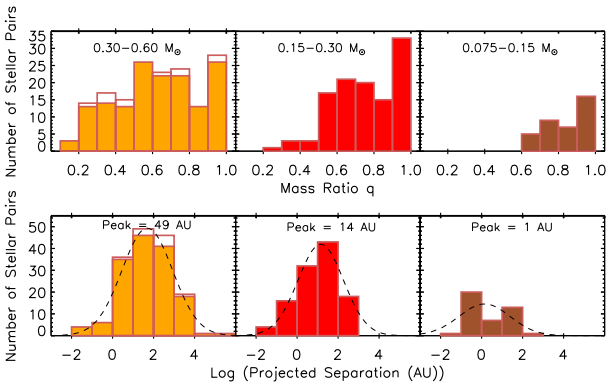

Figure 15. Mass ratios and log-separation distributions for subsamples of M dwarfs as a function of primary masses. *(top left)*: Mass ratios for primaries with masses 0.30–0.60 $M_\odot$ are represented in orange, with the ten multiple systems with primaries more massive than 0.60 $M_\odot$ shown unfilled; *(top middle)*: mass ratios for primaries with masses 0.15–0.30 $M_\odot$ are shown in red; *(top right)*: mass ratios for primaries with masses 0.075–0.15 $M_\odot$ are shown in brown. The axis scales are the same for all three plots to highlight the differences between each mass subsample. The mass ratio ranges shrink as a function of decreasing primary mass in part due to the imposed lower stellar companion mass limit of 0.075 $M_\odot$, although some effect due to gravitational binding energy is likely. *(bottom left)*: the distribution of the projected separations for companions to stars with 0.30–0.60 $M_\odot$, with the ten multiple systems with primaries more massive than 0.60 $M_\odot$ shown unfilled; *(bottom middle)*: the distribution of the projected separations for companions to stars with 0.15–0.30 $M_\odot$; *(bottom right)*: the distribution of the projected separations for companions to stars with 0.075 − 0.15 $M_\odot$. The axis scales are the same for all three plots to highlight the differences between each mass subsample. The peaks of the projected separation distributions shift to closer separations with decreasing primary mass subset.

8.2. *M Dwarf Multiplicity as a Function of Mass and Separation*

Next, we evaluate how the mass of the primary drives the separations at which companions are found. The bottom three panels of Figure 15 show the log-projected separation distributions for the three sample mass subsets. Again, the axis scales are the same between plots, and no substellar or suspected companions are included in these histograms. As in the top row of plots, the number of multiples decreases as a function of primary mass. It is evident that the distribution peaks move to smaller separations as a function of decreasing primary mass,

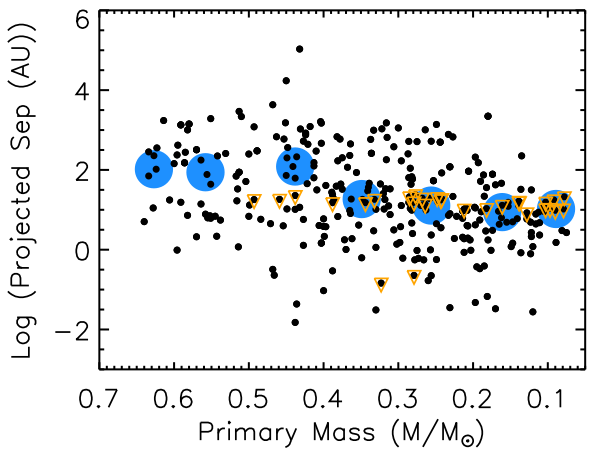

Figure 16. The log of the projected separation in AU as a function of primary mass for the 312 stellar pairs. The more massive M dwarf primaries seem to lack companions at very close separations. A weak trend of decreasing projected separation with primary mass is seen, as emphasized by the large blue points indicating the log of the median projected linear separation, binned by 0.10 $M_\odot$. Pairs with estimated upper limits on their separations have been indicated with inverted orange triangles. The two outliers at very large projected separations from their primaries are G164-042C and GJ0130.1C, both with angular separations from their primaries in the thousands of arcseconds.

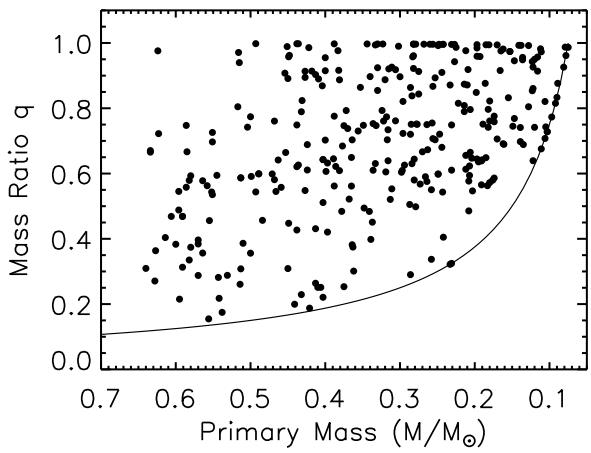

Figure 17. The mass ratios of 312 pairs as a function of primary mass. A trend of mass ratios increasing to unity for low mass primaries is noted. The solid line indicates the mass ratio boundary relative to the lowest mass star considered here for this survey, with M = 0.075 $M_\odot$.

following the trend from solar-type stars to M dwarfs as a whole. Comparison of our distribution peak for the mid-mass sub-sample, which corresponds most closely to the mid-M sample surveyed in Janson et al. (2014a), shows a peak at slightly larger projected separations (14 AU) than the peak reported from their survey (3–10 AU). This discrepancy is expected, as their survey targeted companions at small angular separations.

Rather than using histograms alone, because we have such a large number of companions we can also examine the explicit dependence of separation vs. primary mass, as shown in 16. Each primary-companion projected separation is plotted against the mass of the primary. Blue points represent median values using mass ratio bins of 0.1 $M_\odot$ wide. In orange are highlighted those pairs with upper estimates on their separations that will move to smaller separations once higher resolution observations are obtained. The two outliers at projected separations greater than 10,000 AU are very wide companions that are each part of hierarchical triple systems: G164-042C and GJ0130.1C. Both objects are separated from their primaries by thousands of arcseconds, the largest angular separations in the sample.

Figure 17 shows the mass ratios of all 312 pairs in the sample, as a function of primary mass. We note that the distribution is fairly uniform, with no preference for equal-mass systems. There appear to be a dearth of equal mass companions to the more massive M dwarfs (masses 0.52 – 0.62 $M_\odot$). The apparent trend of mass ratios converging to unity with the decrease in primary mass is expected because we have set a hard limit on companion masses by only including stellar companions, and there is a decreasing amount of mass phase space available as the primary's mass approaches this stellar boundary.

As noted in §5.3, brown dwarf companions have been excluded from the analysis. The percentage of M dwarfs with known brown dwarf companions is 1.3%, a fraction too low to fill in the open region on the graph where low mass primaries have no secondaries at large mass ratios.

The overall trends of Figures 16 and 17 reinforce the result of the histograms in Figure 15 — **lower mass M dwarfs tend to have companions at smaller separations and larger mass ratios than higher mass M dwarfs.**

8.3. *M Dwarf Multiplicity as a Function of Tangential Velocity*

Because it is known that the tangential velocity, v_{tan}, of a star generally increases with age due to gravitational kicks from objects in the Milky Way (usually from Giant Molecular Clouds), cool subdwarfs will generally have larger velocities (e.g., $v_{tan} > 200$ km s^{-1}; Jao et al. 2017) than young stars (estimated to be $v_{tan} < 35$ km

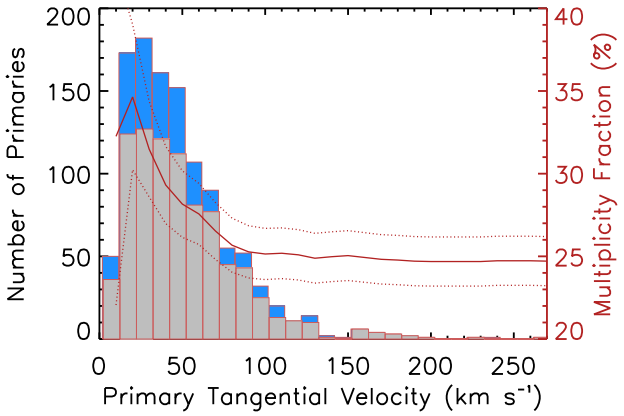

Figure 18. Histogram of primary tangential velocity. The tangential velocity of the primary (or single) component in each system is plotted in gray, with the primaries of confirmed multiple systems indicated in blue. Overplotted in red is the curve of the running multiplicity rate as a function of v_{tan}, indicating that slower moving objects tend to have companions slightly more often. Poisson errors on the multiplicity fraction are indicated by dotted lines.

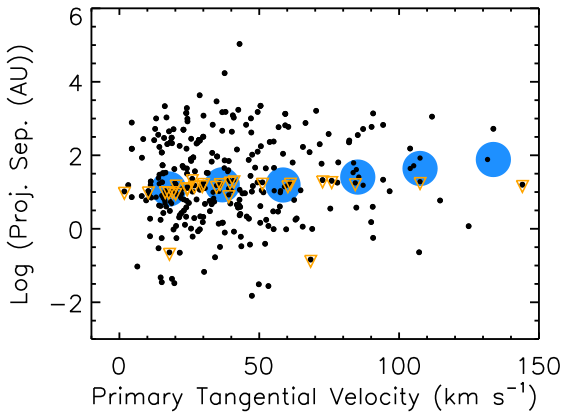

Figure 19. The log of the projected separation in AU as a function of tangential velocity for the 312 stellar pairs. Not shown is the one subdwarf binary with $v_{tan} > 150$ km s^{-1}. A weak trend of increasing projected separation with increasing tangential velocity is seen. This is emphasized by the large blue points indicating the log of the median projected linear separation as a function of the median tangential velocity, in bins of 25 km s^{-1}. Pairs with estimated upper limits on their separations have been indicated with inverted orange triangles. The two outliers at very large projected separations from their primaries are G164-042C and GJ0130.1C, both with angular separations from their primaries in the thousands of arcseconds.

s^{-1}).[16] Thus, we investigate M dwarf multiplicity as a function of v_{tan}, which we use as a proxy for age. Figure 18 shows the v_{tan} distribution of the observed sample, using the v_{tan} of the primary component, where singles are shown in gray and multiples in blue. There are noticeably more multiple systems with $v_{tan} < 50$ km s^{-1} than at larger v_{tan}. The overplotted red curve gives the running multiplicity rate as a function of v_{tan}, showing a general decrease in multiplicity with increasing v_{tan}.[17] This implies that as small stars age and experience kicks in their travels through the Galaxy, they lose companions. Alternately, these older stars may have experienced different multiplicity formation rates at the outset, either because of different (presumably lower) metallicities, or different star formation environments.

Figure 19 further illustrates how multiplicity changes with v_{tan}, showing the log of the projected separation as a function of v_{tan}. The blue open circles represent the log of the median projected separation in 25 km s^{-1} bins, illustrating a weak trend of increasing projected separation with increasing v_{tan}. The orange inverted triangles mark pairs for which the separations are upper limits; these pairs are more numerous at the slower end of the plot, hinting that the median v_{tan} may decrease even further there, once true separations are available for those close pairs. **Thus, the overall trends are that faster moving stars have fewer companions, and that the separations of multiples with higher velocities tend to be larger than their slower-moving counterparts.**

8.4. *Young Stellar Objects*

Within the solar neighborhood are young moving groups that have contributed members to the multiplicity sample. Within the studied collection are sixteen confirmed young M dwarfs, nine of which are known to be multiple, yielding a multiplicity rate of 56 ± 19%. We note that this result is not statistically robust due to the small number of objects with which it was calculated. Presented in Table 13 are these known nearby young red dwarfs, with their astrometric data duplicated from Table 3. In addition, the tangential velocity v_{tan} is listed, along with the youth indicators, the moving group with which they are associated, and the reference. The youth indicators are as follows: BF — a bona fide

[16] This is a 1-σ deviation from the tangential velocity of the oldest nearby young moving group AB Doradus. We consider this a reasonable maximum v_{tan} rate for young stars after comparing the total space motions of the ten nearby young moving groups listed in Table 1 of Mamajek (2016) with ages $\lesssim$ 150 Myr. The mean for all ten (including AB Doradus) is 25 km s^{-1}.

[17] The apparent drop in the MR at $v_{tan} \approx 15$ km s^{-1} is due to the incompleteness of the sample at low proper motions and corresponding v_{tan} values, and is not a real trend.

and well-known member of a moving group; Li — the presence of lithium; ol — over-luminous. Any member of a multiple system where one component exhibits any of these indicators is also assumed to be young, as in the case of GJ 871.1AB.

8.5. *Old, Cool Subdwarfs*

There are a small number of old halo members, also known as cool subdwarfs, that happen to be passing through the solar neighborhood. The objects have been identified either spectroscopically or stand out on a Reduced Proper Motion Diagram. Out of the eleven confirmed subdwarf members with trigonometric parallaxes found within 25 pc, only three are multiple systems, resulting in a multiplicity rate of 27 ± 16%, which is very similar to that of the M dwarf population as a whole. As with the young stars, with such a small number of objects, this result is not statistically robust. A larger sample of 62 K and M subdwarfs has been studied by Jao et al. (2009), who found a rate of of 26 ± 6%. The subdwarfs in our sample are identified in Table 14. In addition to the astrometric data for each system that have been duplicated from Table 3, the calculated tangential velocities v_{tan} and spectral types from the literature are listed.

9. OBSERVATIONAL BIASES & SELECTION EFFECTS

We now address the biases known to have affected this survey. They include (1) a Malmquist bias, (2) selection effects from imposed parallax error limits, (3) missing primaries, particularly from the lowest mass bin, (4) companions at intermediate ρ with large Δmags, and (5) close, unresolved companions at ρ smaller than the sensitivities probed. Each is discussed below, but only the final bias discussed is explicitly corrected in this work.

One criterion for an object's inclusion in the sample of 1120 stars is that it have a trigonometric parallax in order to create a volume-limited collection of M dwarfs. Because brighter objects are generally targeted for parallax measurements before fainter objects for which measurements are more difficult, 85% of the sample is made up of bright stars ($I < 12.00$), introducing an implicit Malmquist bias. As unresolved multiple systems are usually over-luminous, this survey's outcomes are biased toward a larger multiplicity rate.

Because we have required the error on the published trigonometric parallax to be ≤10 mas in order to limit the sample to members that are reliably within 25 pc, it is possible that binaries were missed, as perturbations on the parallax due to an unseen companion can increase the parallax error. Forty-five M dwarf systems with YPC or HIP parallaxes were eliminated from the sample due to their large parallax errors. If all 45 were included in the sample, the sample size would increase to 1165, and if all were found to be multiple, the multiplicity rate would increase by 3.9%. We do not include any correction due to this bias. We note that the parallaxes measured as a result of RECONS' astrometry program, roughly one-third of the sample, would not factor into this negative bias, as all of these data were examined and stars with astrometric perturbations due to unseen companions flagged.

There is mass missing within 25 pc in the form of M dwarf primaries (Winters et al. 2015), the largest incomplete subsample being the lowest mass bin (0.075 − 0.15 $M_\odot$) due to their low luminosities. A conservative estimate of how many of these low mass primaries are missing can be made by assuming that none are missing from the 57 found within 10 pc. Assuming a constant stellar density and extrapolating that value to 25 pc results in an expected number of 891 systems, of which 215 are currently known. This implies that 676 systems are missing from the lowest mass bin of M dwarfs in our sample. That bin also has the smallest (uncorrected) multiplicity rate: 15.8%, (see §8.1 and Figure 14), implying 106 missing multiples. If we add the 676 'missing' systems to the currently known sample of 1120 systems, the 106 new multiples amount to 5.9% that would be missing from the larger collection of 1796 M dwarfs. However, the current uncorrected multiplicity rate of 23.7% for all M dwarfs would decrease to 14.8% with a sample increase to 1796 M dwarf primaries. The addition of the 5.9% from these faint primaries would result in an overall multiplicity rate of 20.7%. We do not include a correction for this bias.

This study was not sensitive to companions with large Δmags at separations ∼1 — 2″, as we show in §4.2.2. The ΔM_I for the M dwarf sequence from M0 to M9.5 spans almost nine magnitudes, with M_I varying from 6.78 — 15.32 mag. While the long exposure $I-$band images obtained during the direct imaging campaign would likely reveal fainter companions at ρ ∼2 — 5″, the saturation of most of the observed stars creates a CCD bleed along columns in the direction in which the CCDs read out. Those faint companions located within ∼1— 2″ of their primaries, but at an orientation near 0° or 180° would be overwhelmed by the CCD bleed of the saturated star to even larger separations and not be detected. This effect would decrease the expected multiplicity rate very slightly. We do not include any correction due to this bias.

Another bias (discussed in §6) is that this study was not uniformly sensitive to 'close' companions found at

Table 13. Young Members

Name	# objects	RA	DEC	μ	P.A.	Ref	v_{tan}	Youth	Moving	Ref
		(hh:mm:ss)	(dd:mm:ss)	($''$ yr^{-1})	(deg)		(km s^{-1})	Indicator	Group	
LTT 10301AB	2	00 50 33.2	+24 49 00	0.199	101.4	4	11	ol	Argus	2
G 80-21	1	03 47 23.3	−01 58 19	0.330	145.8	4	25	Li	AB Dor	2
2MA 0414-0906	1	04 14 17.3	−09 06 54	0.168	325.2	3	19	Li	none	2
LP 776-25	1	04 52 24.4	−16 49 21	0.243	150.7	1	19	ol	AB Dor	2
GJ 2036AB	2	04 53 31.2	−55 51 37	0.153	061.6	4	8	BF	AB Dor	2
LP 717-36AB	2	05 25 41.6	−09 09 12	0.208	164.2	5	20	ol	AB Dor	2
AP COL	1	06 04 52.1	−34 33 40	0.330	003.6	5	13	Li	Argus	2
CD-35 2722AB	2	06 09 19.2	−35 49 30	0.060	184.4	3	6	BF	AB Dor	2
GJ 2060ABC	3	07 28 51.3	−30 14 48	0.185	224.7	4	14	BF	AB Dor	2
GJ 382	1	10 12 17.6	−03 44 44	0.287	211.7	4	11	ol	AB Dor	2
TWA 22AB	2	10 17 27.0	−53 54 27	0.149	264.4	5	15	Li	Beta Pic	2
GJ 393	1	10 28 55.6	+00 50 28	0.947	219.6	4	32	ol	AB Dor	2
GJ 490ABCD	4	12 57 40.2	+35 13 30	0.318	236.3	4	30	BF	Tuc-Hor	2
GJ 856AB	2	22 23 29.1	+32 27 33	0.329	130.2	4	24	Li	AB Dor	2
GJ 871.1AB	2	22 44 57.9	−33 15 01	0.220	123.0	4	24	(Li)	Beta Pic	2
HIP 114066	1	23 06 04.8	+63 55 34	0.181	108.9	4	21	Li	AB Dor	2

NOTE—The youth indicators are as follows: BF — a bona fide and well-known member of a moving group; Li — the presence of lithium; ol — over-luminous.

References—(1) Høg et al. (2000); (2) Riedel et al. (2017); (3) Shkolnik et al. (2012); (4) van Leeuwen (2007); (5) Winters et al. (2015).

separations smaller than $\sim 2''$, so these unresolved multiples will have been missed, resulting in a smaller multiplicity rate. This effect is believed to be the most significant sample bias encountered and has been addressed by studying the nearly completely searched 10 pc sample. As detailed in §6, we have determined that a correction of 2.9% is needed for the stars between 10 — 25 pc.

If we multiply this 2.9% by the number of M dwarf systems in the sample found at distances 10 — 25 pc (933 systems), the number of close multiples missing from the sample amount to 27. However, we have identified 56 candidate multiple systems, 51 of which are currently believed to be single; the other five are already known to have a companion at a large angular separation. An additional four of these 51 candidates have parallaxes placing them within 10 pc, leaving 47 suspected close multiples at distances 10 — 25 pc. If the four candidates within 10 pc are found to be multiple, they would need to be added to the currently known 35 (of 188) M dwarf systems known have companions at angular separations $< 2''$, and the correction factor would increase to 4.9%. The number of close multiples missing at distances 10 — 25 pc would then increase to 46, a number very close to the 51 new suspected multiples that have already been identified.

10. NOTES ON INDIVIDUAL SYSTEMS

There are some systems that require more detail than that given in Table 11, typically those that constitute more than two components or that are particularly interesting. These are listed here with the first four digits of RA and Decl. in sexagesimal hours and degrees, respectively. Note that below, we adopt the moniker GJ to identify all Gl, GL, and GJ stars, also known as "Gliese" stars.

GJ 1003 (0007+2914) Gliese & Jahreiss (1988) claim that GJ 1003 and GJ 1034 are members of the same system. They are separated by ∼16°, with $\mu = 1\farcs89$ yr^{-1}, $\theta = 127°$ for GJ 1003 and $\mu = 1\farcs84$ yr^{-1}, $\theta = 112°$ for GJ 1034, with $\pi = 53.5 \pm 2.5$ mas and

Table 14. Subdwarf Members

Name	# objects	RA	DEC	μ	P.A.	Ref	v_{tan}	Spectral	Ref
		(hh:mm:ss)	(dd:mm:ss)	($''$ yr^{-1})	(deg)		(km s^{-1})	Type	
LHS 1490	1	03 02 06.36	−39 50 51.9	0.859	221.3	8	57	M5.0 VI	4
GJ 1062	1	03 38 15.70	−11 29 13.5	3.033	152.0	7	230	M2.5 VI	3
LHS 189AB	2	04 25 38.35	−06 52 37.0	1.204	145.7	2	105	M3.0 VIJ	4
LHS 272	1	09 43 46.16	−17 47 06.2	1.439	279.2	5	92	M3.0 VI	3
GJ 455AB	2	12 02 18.08	+28 35 14.2	0.791	268.0	7	76	M3.5 VIJ	3
LHS 2852	1	14 02 46.66	−24 31 49.6	0.506	315.6	8	41	M2.0 VI	3
LHS 375	1	14 31 38.25	−25 25 32.9	1.386	269.0	7	158	M4.0 VI	3
SSSPM J1444-2019	1	14 44 20.33	−20 19 25.5	3.507	236.0	6	270	M9.0 VI:	6
GJ 2116	1	15 43 18.33	−20 15 32.9	1.173	195.3	8	119	M2.0 VI	1
LHS 3409	1	18 45 52.24	+52 27 40.6	0.843	298.0	7	81	M4.5 VI	3
LHS 64AB	2	21 07 55.39	+59 43 19.4	2.098	209.0	7	238	M1.5 VIJ	3

References—(1) Bidelman (1985); (2) Costa et al. (2006); (3) Gizis (1997); (4) Jao et al. (2008); (5) Jao et al. (2011); (6) Schilbach et al. (2009); (7) van Altena et al. (1995); (8) Winters et al. (2015).

48.9 ± 4.5 mas, respectively. While their proper motions and distances are similar, this would be the widest separation of any multiple system in the sample, with a projected separation of 5.6 pc. We do not link these two stars as a binary.

GJ 2005ABC (0024-2708) This system is a triple, not a quadruple. Upon further analysis of the *HST-FGS* data, the D component reported in Henry et al. (1999) is a false detection and is not real.

GJ 1046AB (0219-3646) The SB companion is a probable brown dwarf with 168.848 day period (Kürster et al. 2008); also described by Zechmeister et al. (2009). Bonfils et al. (2013) also note that the companion is a brown dwarf or sub-stellar in nature.

GJ 109 (0244+2531) This object is tagged as a VIM (Variability-Induced Mover) in the *Hipparcos* catalog, which could imply duplicity. However, Pourbaix et al. (2003) have shown this to be an incorrect tag in their re-analysis and re-calculation of the $(V-I)$ colors. This object is not included as a candidate multiple.

GJ 165AB (0413+5031) Allen et al. (2007) refer to Gl 165B (what we here call GJ 165B) as an L4 dwarf; however, this is likely a typo for GD 165B, which is reported as a bona fide brown dwarf companion to a white dwarf Kirkpatrick & McCarthy (1994); McLean et al. (2003). The coordinates of GD 165B are α = 14:24:39.09, δ = +09:17:10.4, so it is not the same object as GJ 165B. Kirkpatrick & McCarthy (1994) discuss both Gl 65B and GD 165B, so perhaps that is the source of the confusion. GJ 165AB seems to be a possible equal magnitude binary (Heintz 1992), while McAlister et al. (1987) provide separation information from speckle observations. These data are noted in Table 11.

LTT 11399 (0419+3629) Both Worley (1961) and Worley (1962) claim that this is a binary with a separation of 6.″4 at 226°. Closer inspection and backtracking of its proper motion indicate that the alleged component is a background star. Balega et al. (2007) looked at this star with speckle but were unable to resolve it. It is also marked as having a stochastic solution in Lindegren et al. (1997). We consider this to be a single star and do not list it in Table 12.

GJ 273 (Luyten's Star) (0727+0513) This star was reported in Ward-Duong et al. (2015) as having a close companion; however, based on previous observations of this object with myriad methods (IR speckle (Leinert et al. 1997), long-term astrometric monitoring (15.2 yr Gatewood 2008), high resolution spectroscopy (Nidever et al. 2002; Bonfils et al. 2013), etc.), we conclude that the reported companion must be an unassociated background object. We treat this object as single.

GJ 289 (0748+2022) Marcy & Benitz (1989) mention that Gl 289 (GJ 289) is an SB2, but we believe this is actually a typo for GJ 829, which is an SB2 with an orbit reported in Delfosse et al. (1999a). We did not see reports of GJ 289 being an SB2 noted anywhere else in the literature. We treat GJ 289 as a single object.

GJ 1103 (0751-0000) Reiners et al. (2012) cite Delfosse et al. (1998) for GJ 1103(A) being an SB. However, Delfosse et al. (1998) note only that they exclude GJ 1103 from their sample due to it being a binary. They do not claim that it is an SB. In the LHS Catalog, where it is listed as LHS 1951, it is advertised to have a companion LHS 1952 with a separation of 3″ at θ = 78°, with component magnitudes of m_R = 13.0 and 15.5, and m_{pg} = 15.0 and 17.5. Krupa Ghanda looked for the companion in 2006 by examining (a) RECONS astrometry frames, in which the seeing was sometimes 1.″2 or better, and (b) blinking POSS plates via Aladin. No companion was found. We conclude that GJ 1103 is single.

GJ 450 (1151+3516) This object was reported as a low probability binary candidate with a low velocity amplitude by Young et al. (1987) who measured five epochs of precise radial velocities. However, more recent high resolution observations with ELODIE and SOPHIE over a range of resolutions (R = 40,000 - 75,000) make no mention of this object being multiple (Houdebine 2010), nor was a companion detected with lucky imaging (Jódar et al. 2013) or with infrared adaptive optics observations (Ward-Duong et al. 2015). We therefore consider this object to be single.

GJ 452 (1153−0722) Gould & Chanamé (2004) report a likely white dwarf companion at ρ = 9″ and θ = 110° that was detected in 1960 by Luyten (1980a). However, blinking SuperCOSMOS plate images (epochs 1984 - 1997) with the 300 second integration taken at the CTIO/SMARTS 0.9m reveals no co-moving companion. Backtracking the proper motion of the star to epoch 1960 does place a background star at the appropriate separation and position angle. We thus consider this object to be single.

GJ 1155AB (1216+0258) This object was previously thought to have a white dwarf companion, but Gianninas et al. (2011) report that the white dwarf is actually a misclassified M dwarf. A survey of SDSS objects by Kleinman et al. (2004) did not spectroscopically confirm the companion as a white dwarf. We therefore consider the companion to be an M dwarf.

GJ 465 (1224-1814) Heintz (1986) notes this object may yet be a long-term binary. We note this system as a candidate multiple in Table 12.

GJ 471 (1231+0848) Poveda et al. (1994) claim that this object is a common proper motion companion to the binary GJ 469AB with a separation of 2490″. While the weighted mean trigonometric distances from van Altena et al. (1995) and van Leeuwen (2007) agree within the error bars (73.13 ± 1.28 mas for GJ 471 versus 74.77 ± 3.39 mas for GJ 469AB), their proper motions are significantly different (822 mas yr^{-1} at θ = 231° for GJ 471 versus 685 mas yr^{-1} at θ = 248° for GJ 469AB). Thus, we consider GJ 471 a single star.

GJ 477AB (1235-4556) This object is flagged in the Hipparcos DMSA (Lindegren et al. 1997) as having a stochastic solution, indicating that it is a probable short-period astrometric binary. Zechmeister et al. (2009) note it as an SB1 using VLT+UVES, with the companion being low-mass or a brown dwarf. We treat the companion as a stellar component.

GJ 1167 (1309+2859) Jahreiß et al. (2008) note a B component with μ = 0.″292 yr^{-1}, θ = 234.9°. He then notes that the two stars are not physically associated, as the photometric distance for B is 190 pc while the trigonometric distance for A is 12 pc. We calculate the *ccddist* for A to be 14.2 pc. Janson et al. (2012) note that A is single in their survey. We conclude that GJ 1167'B' is not a CPM companion to GJ 1167A and that GJ 1167 is a single system.

GJ 680 (1735−4840) A companion at ρ = 3.94″, θ = 323.7° with ΔH = 1.93 mag was reported in Ward-Duong et al. (2015). However, whilst performing PSF photometry in the crowded field in order to deblend the magnitudes of the primary and secondary, we noted that the alleged secondary had not moved with the primary between epochs of photometry taken eighteen months apart. With a proper motion of 462 mas yr^{-1}, the two stars would have moved a pixel and a half. This was the case with the primary, but not the alleged secondary. Therefore, we deem the companion a background star and not physically associated.

GJ 687 (1736+6820) Montet et al. (2014) cite Jenkins et al. (2009) for the M3.5 companion that they note in their Table 2. But the spectral type of the *primary* is M3.5. Jenkins et al. (2009) do not note any additional information about a companion.

We find that the WDS lists GJ 687 as the B component to the F5 star HD 160861. The parallax for the F5 star is 11.20 mas (89 pc; van Leeuwen 2007) which places this object at a much larger distance than the M dwarf, which has π = 220.47 mas (corresponding to 4.5 pc; van Altena et al. 1995; van Leeuwen 2007). It appears that the 'A' component, the F5 star (at α = 17:36:42, δ = +68:22:59, compared to α = 17:36:25.9, δ = +68:20:20 for GJ 687) is an SB, for which the measurement by McAlister et al. (1987) pertains. Tokovinin (1992) notes GJ 687 as both an astrometric and speckle binary in the table in that paper named 'Long-period spectroscopic binaries'. But this, too, is likely for the F dwarf. The companion is deemed to be optical, and presumably GJ 687 is single.

LTT 15769 (1945+3223) This system is listed as double in the *Hipparcos* DMSA (Lindegren et al. 1997) with $\rho = 12\farcs76$, $\theta = 339°$ with a quality code of 'D', indicating an uncertain solution. Blinking the SuperCOSMOS R plate image with an I-band image taken with the Lowell 42in image results in an epoch difference of nineteen years and reveals the motion of the primary, but not that of the bright 'secondary' with a ΔH_p of 2.3 mag. We thus refute this low probability companion and deem the system 'single.'

GJ 793 (2030+6527) Weis (1991b) lists this object in his 'Rejected Pairs' table (Table 5) and notes that the alleged companion is not listed in either the Luyten or Giclas catalogs. The SuperCOSMOS plates had an epoch spread of only one year, so we used the 300-second image taken during our imaging campaign at the Lowell 42in to blink with the SuperCOSMOS $I-$band archival image. This resulted in a δt = 20 yr. No common proper motion companion was detected. We confirm that this object is single.

GJ 873 (2246+4420) This object was reported by van de Kamp & Worth (1972) to be an astrometric binary, but this detection was later found to be due to systemmatic errors in the micrometric separation measurements (Heintz 1976).

Young et al. (1987) initially report this object as a high probability SB1, but then note in the appendix to that paper that the detection is tentative due to the low velocity amplitude of the signal.

Hełminiak et al. (2009) also investigate this system, citing a 'B' component that they infer is a real binary with spectral type G, but not associated with the 'A' component, our M dwarf. We confirm by blinking that the two are not physically bound, as the G dwarf binary has a very different proper motion (α_μ = 8.6 mas, δ_μ = -2.0 mas) from that of the M dwarf component (α_μ = -705 mas, δ_μ = -461 mas), and thus the two systems do not move together. Also, the V magnitudes for the two 'components' are not physically possible if they are located at similar distances: the M dwarf has $V = 10.22$, while the G dwarf has $V = 10.66$.

Tanner et al. (2010) report two unconfirmed companions found via AO, but the two candidates are too faint to have 2MASS magnitudes available.

Finally, Docobo et al. (2010) observed this object using speckle interferometry on a 6m telescope and did not resolve a companion. They were able to resolve companions down to angular separations of 22 mas, corresponding to 0.11 AU at the object's distance of 5 pc.

We consider this object to be a single star.

11. DISCUSSION

We now put the results from this survey in perspective by making comparisons to results from other M dwarf multiplicity surveys, as well as to surveys of more massive stars. We then discuss how unresolved companions affect the red dwarf luminosity and mass distributions. Finally, directions for future work will be outlined.

11.1. *Comparison to Other M Dwarf Surveys*

As noted in §1, previous surveys have been done to determine M dwarf multiplicity, but most have studied samples on the order of a hundred stars. Some of the surveys (Skrutskie et al. 1989; Delfosse et al. 1999a) did not report a multiplicity rate in their results, so they will not be addressed. Others explored the regions around M dwarfs in search of different types of objects (brown dwarfs in the case of Dieterich et al. (2012) and Jovian mass planets in the case of Endl et al. (2006)) or at different separation regimes (Dhital et al. (2010) and Law et al. (2010) explored only the wide binary rate) and are thus not relevant to the present comparison. For example, searches for substellar objects can be provide lower limits for the types of companions found around M dwarfs, but stellar companions are not always reported. Law et al. (2006, 2008) probed different sample sizes of late-type M dwarfs using the lucky imaging and report multiplicity rates that are different from each other by a factor of two, but still within their large errors. We note that the multiplicity rate calculated here for the lowest mass bin of M dwarfs — 15.8 ± 2.6% — agrees with that reported in Law et al. (2008): 13.6 $^{+6.5}_{-4}$%.

A number of the other samples studied for M dwarf multiplicity determination were volume-limited. Henry & McCarthy (1990) searched the 5 pc sample of M dwarfs, while Henry (1991) and Simons et al. (1996) extended the volume searched to 8 pc. Fischer & Marcy (1992) searched a varied sample of M dwarfs within 20 pc. The samples of Bergfors et al. (2010), Janson et al. (2012), and Janson et al. (2014a) were all within 52 pc, but most distances were photometric parallaxes.

We find that our multiplicity rate result agrees with most of the more recent surveys: Bergfors et al. (2010), Janson et al. (2012), and Janson et al. (2014a) report MRs of 32%, 27%, and 21 — 27%, respectively. Our results also agree with the earlier studies of Henry & McCarthy (1990) and Henry (1991) (34% and 20%) within the errors, but are smaller than the studies of Fischer & Marcy (1992) and Simons et al. (1996) (42% and 40%). It is likely that some of the earlier studies simply did not have enough targets from which to calculate accurate results with low statistical errors.

The only other sizeable survey that was volume-limited and had trigonometric parallaxes available was that of Ward-Duong et al. (2015); however, their sample included late K dwarfs and did not include any late M dwarfs. We find a slightly larger multiplicity rate than the 23.5±3.2% of Ward-Duong et al. (2015), although results agree within the errors. Examination of the sample studied here reveals an additional 308 M dwarfs with parallaxes from sources other than van Leeuwen (2007) that place them within 15 pc, 247 of which are within the color-limits of their sample ($3.65 < (V-K) \lesssim 6.8$).[18]

Due to all of the targets in our multiplicity sample having accurate trigonometric parallaxes, the study presented here has a number of advantages over ones conducted by others. All of the targets considered were reliably known to be within 25 pc. Because we measured VRI photometry for almost all targets lacking it, we were able to use a homogeneous set of data on the same photometric system, combined with the existing parallaxes, to calculate M_V and thus, estimate masses. Most other surveys were forced to use less accurate types of distances to draw conclusions from their data. We were also able to calculate projected separations that were more accurate than those of others, as our sample has trigonometric distances. Finally, our survey was comprehensive in two search regimes, while also able to infer the presence of candidate companions using other methods.

11.2. *Comparison to More Massive Stars*

Listed in Table 15 are the multiplicity statistics for stars of other main sequence spectral types, along with the percentages of all stars by that spectral type. While brown dwarfs are not main sequence objects, they have been included for comparison. The percentage of stars that they comprise has been purposely left blank, as they are not stars, and in fact the size of the brown dwarf population is not well constrained.

While the multiplicity rate decreases as a function of primary mass, it is evident that the number of stars increases with decreasing mass. Massive stars of types OBA are the most rare, accounting for fewer than 1% of all stars (Binney & Merrifield 1998), while solar-type FGK stars make up ∼21% of all stars (Binney & Merrifield 1998). The M dwarfs make up 75% of all stars; thus, their multiplicity statistics have the largest impact. The K dwarf multiplicity rate is the most uncertain, with no comprehensive multiplicity search having yet been done for that spectral type, although efforts to remedy this are currently underway by members of the RECONS group. The thorough study presented here provides an anchor for the statistics at the low end of the stellar main sequence, enabling a complete picture of stellar multiplicity.

Figure 20 indicates the multiplicity rates for dwarf stars, with values taken from the literature for the more massive main sequence stars. The clear decrease in multiplicity with decreasing primary mass is evident.

From this comprehensive picture of stellar multiplicity, we can determine the multiplicity rate of all star systems. Consider one million stars. Table 16 duplicates the percentages of stars for each main sequence spectral type and the multiplicity rate for each of those spectral types from Table 15. In addition, however, is listed the number of stars per one million that each spectral type would contribute and how many of those would be multiple. The extra three percent of stars not shown in the second column are made up of giants, supergiants, and white dwarfs (Binney & Merrifield 1998). Based on the numbers presented, we can conclude that the multiplic-

Table 15. Multiplicity of Main Sequence Stars

Spectral Type	% of Stars	Ref	Mult. Rate	Comp Rate	Ref
O	<0.1	2	>80	130	5,3
B	0.1	2	>70	100	6,3
A	0.6	2	>70	100	6,3
F	3.3	2	50 ± 4	75	6
G	7.8	2	46 ± 2	75	6
K	10.2	2	41 ± 3	56	6
M	75.0	4	26.1 ± 1.4	28	1
L,T	···		22	22	3

NOTE—The columns indicate the spectral type of object, the percentage of stars that each spectral type comprises, along with the reference. Next, the Multiplicity Rate, the Companion Rate and the reference are listed.

References—(1) this work; (2) Binney & Merrifield (1998); (3) Duchêne & Kraus (2013); (4) Henry et al. (2006); (5) Mason et al. (2009); (6) Raghavan et al. (2010).

[18] This red limit has been estimated from the color-color diagram in Figure 1 in their paper, as it is not specified.

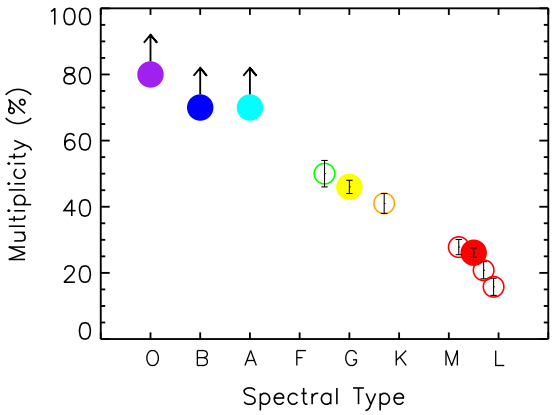

Figure 20. Multiplicity rate as a function of spectral type. Shown is the MR for dwarf stars, with the rates for M dwarfs presented here in red. Open red points are the uncorrected MRs for the three mass bins explored throughout this paper, while the solid point is the total corrected MR for all M dwarfs. Values for stars more massive than M dwarfs are taken from the literature, as listed in Table 15. The open green and orange points are the blue and red subsamples from Raghavan et al. (2010), while the solid yellow point is the average reported in that paper. The arrows indicate the MRs that are likely lower limits. We do not include the L dwarfs here. Clearly, the MR is a function of decreasing mass.

Table 16. Multiplicity Example

Spectral Type	% of Stars	# of Stars	Mult. Rate	# Mult.
O	0.003	30	80	24
B	0.1	1,000	70	700
A	0.6	6,000	70	4,200
F	3.3	33,000	50	16,500
G	7.8	78,000	46	35,880
K	10.2	102,000	41	41,820
M	75.0	750,000	26.1	195,750
	97.0	970,030	30	294,874

ity rate of all main sequence star systems is 30%, and that therefore, most stellar systems are single.

11.3. *The Luminosity and Mass Distributions*

Shown in Figure 21 are luminosity distributions for our sample in M_V, calculated both before (top) and after (bottom) deblending 'joint' photometry with contributions from close companions. Primaries are indicated in red, while companions are shown in blue. The vertical lines at M_V = 9.25, 11.80, and 13.86 correspond to masses of 0.60, 0.30, and 0.15 $M_\odot$ and indicate the divisions by factors of two in mass used to further divide the 25 pc sample for the analysis presented in 8.1. It is evident that a substantial number of companions was hiding in the blended photometry of the M dwarf primaries.

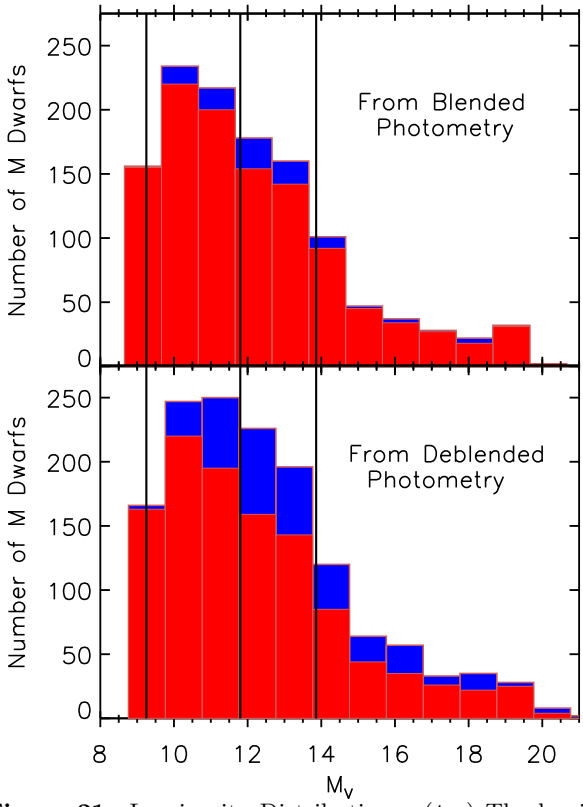

Figure 21. Luminosity Distributions. (*top*) The luminosity distribution for the 1214 M dwarfs in the sample with individual photometry. M_V has been calculated from the blended photometry. (*bottom*) The luminosity distribution for all 1432 M dwarf primaries and secondaries in the sample with M_V calculated from deblended photometry. Primaries are plotted in red; companions in blue. The vertical lines denote the subdivisions by factors of two in mass explored throughout the study. The contributions from the companions in the deblended luminosity distribution are greater than in the blended luminosity distribution.

Figure 22 illustrates the mass distribution for the 1212 M dwarfs with individual photometry with masses calculated from blended photometry (top) and the distribution for all 1432 M dwarf components (primaries plus all secondaries) found within 25 pc in the survey after deblending photometry (bottom). Both histograms show a gentle, but steady rise to the end of the stellar

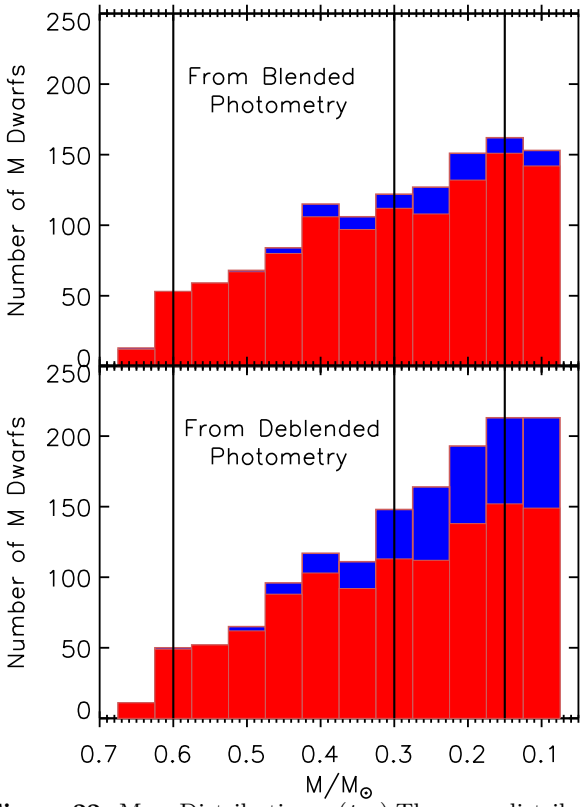

Figure 22. Mass Distributions. (*top*) The mass distribution for the 1212 M dwarfs in the sample with masses estimated from blended photometry. (*bottom*) The mass distribution for all 1432 M dwarfs in the sample with masses estimated from deblended photometry. Primaries are plotted in red; stellar companions in blue. The vertical lines denote the subdivisions by factors of two in mass explored throughout the study. There is a noticeable difference in the shapes of the distributions, as the contributions to the low mass companions contribute to the rise of the mass distribution to the end of the main sequence.

main sequence, what we have defined to be 0.075 $M_\odot$. This trend is emphasized by the additions of the companions in each histogram, as they are all lower masses than their primaries, by definition.

11.4. *Mass Contributions from Primaries and Hidden Companions*

We now consider the contributions to the Galactic mass budget by M dwarfs. Without any prior knowledge of unresolved companions, a naive estimate of the mass of the 1212 M dwarfs in the sample with indivdually measured photometry, from which masses are estimated, yields 364 $M_\odot$. This includes the 1120 M dwarf primaries plus their 92 well-separated secondaries.

However, of the 265 primaries in the sample of multiples, 210 have 257 companions located at angular separations of less than 2″ from either their primaries or their widely separated secondaries, resulting in 'joint', or blended, V magnitudes. After deblending, we find that the 1120 primaries contribute 335$_\odot$. The deblended companions have added 38$M_\odot$ to the total M dwarf mass, indicating that 10% was hidden as unresolved stars. We find that at least 17% (67 $M_\odot$/402 $M_\odot$) of M dwarf mass is found in companions, with unresolved companions contributing at least 57% (38 $M_\odot$/67 $M_\odot$) of the companion mass and donating 9% (38 $M_\odot$/402 $M_\odot$) to the total mass budget of M dwarfs. We emphasize that these values are all lower limits, as this collection of M dwarfs has not been thoroughly canvassed for companions at separations of less than 2″, where most M dwarf companions are found.

12. SUMMARY OF RESULTS

• We report 20 new and 56 suspected companions to M dwarfs within 25 pc;

• We find a corrected multiplicity rate of 26.1±1.4% for M dwarfs;

• We find the uncorrected multiplicity rate of the three mass subsets (0.30 — 0.60 M/$M_\odot$, 0.15 — 0.30 M/$M_\odot$, and 0.075 — 0.15 M/$M_\odot$) to be 27.8 ± 2.3%, 20.8 ± 2.6%, and 15.8 ± 2.6%, with a hint that multiple systems have yet to be discovered for the least massive bin;

• The mass ratios for the mass sub-samples show weak rises that lead to a more compelling rise to equal mass ratios for the entire M dwarf multiplicity sample;

• The distribution of the projected separations of the companions peaks at 20 AU, i.e., the scale of the outer Solar System;

• We calculate the corrected multiplicity rates for the three angular separation regimes (< 2″, 2 — 10″, and > 10″) to be 18.5 ± 1.2%, 3.5 ± 0.6%, and 4.6 ± 0.6%;

• A weak trend of decreasing projected separation with primary mass was found;

• Analysis of the tangential velocities of the primaries reveals a possible relation between multiplicity and tangential velocity, indicating that older, faster moving M dwarfs tend to have fewer companions as a population than their younger counterparts;

• We find that at least 17% of M dwarf mass is contained in companions, with 9% of the total mass budget made up of 'hidden' stellar companions;

• Finally, we demonstrate that the mass distribution of our volume-limited sample rises to the end of the stellar main sequence.

13. WHAT IS YET TO COME

While the multiplicity survey presented here was comprehensive for stellar companions to M dwarfs with sep-

arations 2 – 300″, much work remains to be done. Currently underway are high-resolution speckle imaging and radial velocity studies to probe within 2″ of these nearby M dwarfs in order to complete our understanding of M dwarf multiplicity at all separation regimes. The results from these ongoing surveys will provide the separation and delta-magnitude measurements needed for a more thorough understanding of the characteristics of these multiple systems, e.g., the mass ratio and separation distributions. In addition, the radial velocities being measured provide the third velocity component needed to calculate precise UVW space motions. These space motions will allow further exploration of the possible trend of stellar multiplicity with tangential velocity.

Gaia will have five years or more of exquisite astrometric measurements that will enable the detection of binaries. Any astrometric binary orbits should provide inclinations, and thus the dynamical masses of each component when combined with ground-based spectroscopic orbits. In addition, *Gaia* should reveal many of the very low-mass stars that have escaped detection to-date, providing a more complete picture of the nearby M dwarf population.

14. ACKNOWLEDGMENTS

This work was made possible by National Science Foundation (NSF) grants 09-08402, 0507711, 1109445, and 141206, Sigma Xi Grants-In-Aid-of-Research, the generous budget allotment of Georgia State University that made possible access to the SMARTS telescopes at CTIO and Lowell, and the Georgia State University Dissertation grant. We also thank the members of the SMARTS Consortium, who have enabled the operations of the small telescopes at CTIO since 2003, as well as observers and observer support at CTIO, specifically Arturo Gomez, Mauricio Rojas, Hernan Tirado, Joselino Vasquez, Alberto Miranda, and Edgardo Cosgrove. We are indebted to the support staff and astronomers at Lowell Observatory for their assistance, particularly Len Bright, Larry Wasserman, Brian Skiff, and Ted Dunham.

JGW was supported by a grant from the John Templeton Foundation for a portion of the time that it took to finalize these results. The opinions expressed here are those of the authors and do not necessarily reflect the views of the John Templeton Foundation.

Data products from the Two Micron All Sky Survey, which is a joint project of the University of Massachusetts and the Infrared Processing and Analysis Center/California Institute of Technology, funded by the National Aeronautics and Space Administration (NASA) and the NSF have been used extensively, as have the SIMBAD database and the Aladin and Vizier interfaces, operated at CDS, Strasbourg, France. This work has made ample use of the Smithsonian Astrophysical Observatory/NASA Astrophysics Data System.

JGW extends a heartfelt thanks to David Fanning for the availability of his IDL Coyote Graphics System.

JGW is especially grateful to Jonathan Irwin, Willie Torres, and Eric Mamajek for illuminating and clarifying discussions and suggestions and to Douglas Gies, Harold McAlister, Russel White, Sebastièn Lèpine and David Charbonneau for constructive comments. JGW would also like to thank Brian Mason for access to the Washington Double Star Catalog, a copy of which is housed at Georgia State University.

REFERENCES

Al-Shukri, A. M., McAlister, H. A., Hartkopf, W. I., Hutter, D. J., & Franz, O. G. 1996, AJ, 111, 393

Allen, P. R., Koerner, D. W., McElwain, M. W., Cruz, K. L., & Reid, I. N. 2007, AJ, 133, 971

Allen, P. R., & Reid, I. N. 2008, AJ, 135, 2024

Andrei, A. H., Smart, R. L., Penna, J. L., et al. 2011, AJ, 141, 54

Anglada-Escudé, G., Boss, A. P., Weinberger, A. J., et al. 2012, ApJ, 746, 37

Balega, I. I., Balega, Y. Y., Gasanova, L. T., et al. 2013, Astrophysical Bulletin, 68, 53

Balega, I. I., Balega, Y. Y., Maksimov, A. F., et al. 2007, Astrophysical Bulletin, 62, 339

Bartlett, J. L., Lurie, J. C., Riedel, A., et al. 2017, AJ, 154, 151

Benedict, G. F., McArthur, B. E., Franz, O. G., Wasserman, L. H., & Henry, T. J. 2000, AJ, 120, 1106

Benedict, G. F., McArthur, B., Chappell, D. W., et al. 1999, AJ, 118, 1086

Benedict, G. F., McArthur, B. E., Franz, O. G., et al. 2001, AJ, 121, 1607

Benedict, G. F., McArthur, B. E., Forveille, T., et al. 2002, ApJL, 581, L115

Benedict, G. F., Henry, T. J., Franz, O. G., et al. 2016, AJ, 152, 141

Bergfors, C., Brandner, W., Janson, M., et al. 2010, A&A, 520, A54

Bertin, E. 2011, in Astronomical Society of the Pacific Conference Series, Vol. 442, Astronomical Data Analysis Software and Systems XX, ed. I. N. Evans, A. Accomazzi, D. J. Mink, & A. H. Rots, 435

Bertin, E., & Arnouts, S. 1996, A&AS, 117, 393

Bessel, M. S. 1990, A&AS, 83, 357

Bessell, M. S. 1991, AJ, 101, 662

Beuzit, J.-L., Ségransan, D., Forveille, T., et al. 2004, A&A, 425, 997

Bidelman, W. P. 1985, ApJS, 59, 197

Biller, B. A., & Close, L. M. 2007, ApJL, 669, L41

Biller, B. A., Kasper, M., Close, L. M., Brandner, W., & Kellner, S. 2006, ApJL, 641, L141

Binney, J., & Merrifield, M. 1998, Galactic Astronomy (Princeton University Press)

Blake, C. H., Charbonneau, D., White, R. J., et al. 2008, ApJL, 678, L125

Bonfils, X., Delfosse, X., Udry, S., et al. 2013, A&A, 549, A109

Bonnefoy, M., Chauvin, G., Dumas, C., et al. 2009, A&A, 506, 799

Bowler, B. P., Liu, M. C., Shkolnik, E. L., & Tamura, M. 2015, ApJS, 216, 7

Burningham, B., Pinfield, D. J., Leggett, S. K., et al. 2009, MNRAS, 395, 1237
Caballero, J. A. 2009, A&A, 507, 251
Chanamé, J., & Gould, A. 2004, ApJ, 601, 289
Cortes-Contreras, M., Caballero, J. A., & Montes, D. 2014, The Observatory, 134, 348
Costa, E., & Méndez, R. A. 2003, A&A, 402, 541
Costa, E., Méndez, R. A., Jao, W.-C., et al. 2005, AJ, 130, 337
—. 2006, AJ, 132, 1234
Cvetković, Z., Pavlović, R., & Boeva, S. 2015, AJ, 149, 150
Daemgen, S., Siegler, N., Reid, I. N., & Close, L. M. 2007, ApJ, 654, 558
Dahn, C. C., Harrington, R. S., Riepe, B. Y., et al. 1982, AJ, 87, 419
Dahn, C. C., Harrington, R. S., Kallarakal, V. V., et al. 1988, AJ, 95, 237
Dahn, C. C., Harris, H. C., Vrba, F. J., et al. 2002, AJ, 124, 1170
Davison, C. L., White, R. J., Jao, W.-C., et al. 2014, AJ, 147, 26
Dawson, P. C., & De Robertis, M. M. 2005, PASP, 117, 1
Deacon, N. R., & Hambly, N. C. 2001, A&A, 380, 148
Deacon, N. R., Hambly, N. C., & Cooke, J. A. 2005a, A&A, 435, 363
Deacon, N. R., Hambly, N. C., Henry, T. J., et al. 2005b, AJ, 129, 409
Delfosse, X., Forveille, T., Beuzit, J.-L., et al. 1999a, A&A, 344, 897
Delfosse, X., Forveille, T., Perrier, C., & Mayor, M. 1998, A&A, 331, 581
Delfosse, X., Forveille, T., Udry, S., et al. 1999b, A&A, 350, L39
Dhital, S., West, A. A., Stassun, K. G., & Bochanski, J. J. 2010, AJ, 139, 2566
Díaz, R. F., González, J. F., Cincunegui, C., & Mauas, P. J. D. 2007, A&A, 474, 345
Dieterich, S. B., Henry, T. J., Golimowski, D. A., Krist, J. E., & Tanner, A. M. 2012, AJ, 144, 64
Dieterich, S. B., Henry, T. J., Jao, W.-C., et al. 2014, AJ, 147, 94
Docobo, J. A., Tamazian, V. S., Balega, Y. Y., & Melikian, N. D. 2006, AJ, 132, 994
—. 2010, AJ, 140, 1078
Doyle, J. G., & Butler, C. J. 1990, A&A, 235, 335
Duchêne, G., & Kraus, A. 2013, ARA&A, 51, 269
Dupuy, T. J., & Liu, M. C. 2012, ApJS, 201, 19
Duquennoy, A., & Mayor, M. 1988, A&A, 200, 135
Endl, M., Cochran, W. D., Kürster, M., et al. 2006, ApJ, 649, 436
Fabricius, C., & Makarov, V. V. 2000, A&AS, 144, 45
Faherty, J. K., Burgasser, A. J., Walter, F. M., et al. 2012, ApJ, 752, 56
Falin, J. L., & Mignard, F. 1999, A&AS, 135, 231
Femenía, B., Rebolo, R., Pérez-Prieto, J. A., et al. 2011, MNRAS, 413, 1524
Fischer, D. A., & Marcy, G. W. 1992, ApJ, 396, 178
Forveille, T., Beuzit, J.-L., Delorme, P., et al. 2005, A&A, 435, L5
Frankowski, A., Jancart, S., & Jorissen, A. 2007, A&A, 464, 377
Freed, M., Close, L. M., & Siegler, N. 2003, ApJ, 584, 453
Fu, H.-H., Hartkopf, W. I., Mason, B. D., et al. 1997, AJ, 114, 1623
Gatewood, G. 2008, AJ, 136, 452
Gatewood, G., & Coban, L. 2009, AJ, 137, 402
Gatewood, G., Coban, L., & Han, I. 2003, AJ, 125, 1530
Gatewood, G., de Jonge, K. J., & Stephenson, B. 1993, PASP, 105, 1101
Gershberg, R. E., Katsova, M. M., Lovkaya, M. N., Terebizh, A. V., & Shakhovskaya, N. I. 1999, A&AS, 139, 555
Gianninas, A., Bergeron, P., & Ruiz, M. T. 2011, ApJ, 743, 138
Gizis, J. E. 1997, AJ, 113, 806
—. 1998, AJ, 115, 2053
Gizis, J. E., Reid, I. N., & Hawley, S. L. 2002, AJ, 123, 3356
Gliese, W., & Jahreiss, H. 1988, Ap&SS, 142, 49
Golimowski, D. A., Leggett, S. K., Marley, M. S., et al. 2004, AJ, 127, 3516
Gould, A., & Chanamé, J. 2004, ApJS, 150, 455
Graham, J. A. 1982, PASP, 94, 244
Gray, R. O., Corbally, C. J., Garrison, R. F., McFadden, M. T., & Robinson, P. E. 2003, AJ, 126, 2048
Harlow, J. J. B. 1996, AJ, 112, 2222
Harrington, R. S., & Dahn, C. C. 1980, AJ, 85, 454
Harrington, R. S., Kallarakal, V. V., Christy, J. W., et al. 1985, AJ, 90, 123
Harrington, R. S., Dahn, C. C., Kallarakal, V. V., et al. 1993, AJ, 105, 1571
Hartkopf, W. I., Tokovinin, A., & Mason, B. D. 2012, AJ, 143, 42
Hawley, S. L., Gizis, J. E., & Reid, I. N. 1996, AJ, 112, 2799
Heintz, W. D. 1976, MNRAS, 175, 533
—. 1985, ApJS, 58, 439
—. 1986, AJ, 92, 446
—. 1987, ApJS, 65, 161
—. 1990, ApJS, 74, 275
—. 1991, AJ, 101, 1071
—. 1992, ApJS, 83, 351

—. 1993, AJ, 105, 1188
—. 1994, AJ, 108, 2338
Hełminiak, K. G., Konacki, M., Kulkarni, S. R., & Eisner, J. 2009, MNRAS, 400, 406
Henry, T. J. 1991, PhD thesis, Arizona Univ., Tucson.
Henry, T. J., Franz, O. G., Wasserman, L. H., et al. 1999, ApJ, 512, 864
Henry, T. J., Ianna, P. A., Kirkpatrick, J. D., & Jahreiss, H. 1997, AJ, 114, 388
Henry, T. J., Jao, W.-C., Subasavage, J. P., et al. 2006, AJ, 132, 2360
Henry, T. J., & McCarthy, Jr., D. W. 1990, ApJ, 350, 334
Henry, T. J., Subasavage, J. P., Brown, M. A., et al. 2004, AJ, 128, 2460
Henry, T. J., Jao, W.-C., Winters, J. G., et al. 2018, ArXiv e-prints, arXiv:1804.07377
Hershey, J. L., & Taff, L. G. 1998, AJ, 116, 1440
Høg, E., Fabricius, C., Makarov, V. V., et al. 2000, A&A, 355, L27
Horch, E. P., Bahi, L. A. P., Gaulin, J. R., et al. 2012, AJ, 143, 10
Horch, E. P., Falta, D., Anderson, L. M., et al. 2010, AJ, 139, 205
Horch, E. P., Gomez, S. C., Sherry, W. H., et al. 2011a, AJ, 141, 45
Horch, E. P., Robinson, S. E., Meyer, R. D., et al. 2002, AJ, 123, 3442
Horch, E. P., van Altena, W. F., Howell, S. B., Sherry, W. H., & Ciardi, D. R. 2011b, The Astronomical Journal, 141, 180
Horch, E. P., van Belle, G. T., Davidson, Jr., J. W., et al. 2015a, AJ, 150, 151
Horch, E. P., Veillette, D. R., Baena Gallé, R., et al. 2009, AJ, 137, 5057
Horch, E. P., van Altena, W. F., Demarque, P., et al. 2015b, AJ, 149, 151
Horch, E. P., Casetti-Dinescu, D. I., Camarata, M. A., et al. 2017, AJ, 153, 212
Houdebine, E. R. 2010, MNRAS, 407, 1657
Howell, S. B. 2000, Handbook of CCD Astronomy (Cambridge University Press)
—. 2012, PASP, 124, 263
Ianna, P. A., Patterson, R. J., & Swain, M. A. 1996, AJ, 111, 492
Ireland, M. J., Kraus, A., Martinache, F., Lloyd, J. P., & Tuthill, P. G. 2008, ApJ, 678, 463
Jahreiß, H., Meusinger, H., Scholz, R.-D., & Stecklum, B. 2008, A&A, 484, 575
Jancart, S., Jorissen, A., Babusiaux, C., & Pourbaix, D. 2005, A&A, 442, 365
Janson, M., Bergfors, C., Brandner, W., et al. 2014a, ApJ, 789, 102
Janson, M., Hormuth, F., Bergfors, C., et al. 2012, ApJ, 754, 44
Janson, M., Bergfors, C., Brandner, W., et al. 2014b, ApJS, 214, 17
Jao, W.-C., Henry, T. J., Beaulieu, T. D., & Subasavage, J. P. 2008, AJ, 136, 840
Jao, W.-C., Henry, T. J., Subasavage, J. P., et al. 2003, AJ, 125, 332
—. 2005, AJ, 129, 1954
—. 2014, AJ, 147, 21
—. 2011, AJ, 141, 117
Jao, W.-C., Henry, T. J., Winters, J. G., et al. 2017, AJ, 154, 191
Jao, W.-C., Mason, B. D., Hartkopf, W. I., Henry, T. J., & Ramos, S. N. 2009, AJ, 137, 3800
Jenkins, J. S., Ramsey, L. W., Jones, H. R. A., et al. 2009, ApJ, 704, 975
Jódar, E., Pérez-Garrido, A., Díaz-Sánchez, A., et al. 2013, MNRAS, 429, 859
Khovritchev, M. Y., Izmailov, I. S., & Khrutskaya, E. V. 2013, MNRAS, 435, 1083
Kilkenny, D., Koen, C., van Wyk, F., Marang, F., & Cooper, D. 2007, MNRAS, 380, 1261
Kirkpatrick, J. D., & McCarthy, Jr., D. W. 1994, AJ, 107, 333
Kleinman, S. J., Harris, H. C., Eisenstein, D. J., et al. 2004, ApJ, 607, 426
Koen, C., Kilkenny, D., van Wyk, F., Cooper, D., & Marang, F. 2002, MNRAS, 334, 20
Koen, C., Kilkenny, D., van Wyk, F., & Marang, F. 2010, MNRAS, 403, 1949
Köhler, R., Ratzka, T., & Leinert, C. 2012, A&A, 541, A29
Kraus, A. L., Ireland, M. J., Huber, D., Mann, A. W., & Dupuy, T. J. 2016, AJ, 152, 8
Kürster, M., Endl, M., & Reffert, S. 2008, A&A, 483, 869
Kürster, M., Zechmeister, M., Endl, M., & Meyer, E. 2009, The Messenger, 136, 39
Lampens, P., Strigachev, A., & Duval, D. 2007, A&A, 464, 641
Landolt, A. U. 1992, AJ, 104, 372
—. 2007, AJ, 133, 2502
—. 2009, AJ, 137, 4186
—. 2013, AJ, 146, 131
Law, N. M., Dhital, S., Kraus, A., Stassun, K. G., & West, A. A. 2010, ApJ, 720, 1727
Law, N. M., Hodgkin, S. T., & Mackay, C. D. 2006, MNRAS, 368, 1917
—. 2008, MNRAS, 384, 150

Leinert, C., Henry, T., Glindemann, A., & McCarthy, Jr., D. W. 1997, A&A, 325, 159
Leinert, C., Weitzel, N., Richichi, A., Eckart, A., & Tacconi-Garman, L. E. 1994, A&A, 291, L47
Lèpine, S., & Shara, M. M. 2005, AJ, 129, 1483
Lèpine, S., Thorstensen, J. R., Shara, M. M., & Rich, R. M. 2009, AJ, 137, 4109
Lindegren, L., Mignard, F., Söderhjelm, S., et al. 1997, A&A, 323, L53
Lurie, J. C., Henry, T. J., Jao, W.-C., et al. 2014, AJ, 148, 91
Luyten, W. J. 1979a, LHS Catalogue. Second edition. (University of Minnesota)
—. 1979b, NLTT catalogue. Volume I. +90 to +30. Volume II. +30 to 0. (University of Minnesota)
—. 1980a, NLTT Catalogue. Volume III. 0 to -30. (University of Minnesota)
—. 1980b, NLTT Catalogue. Volume IV. -30 to -90. (University of Minnesota)
Makarov, V. V., Zacharias, N., & Hennessy, G. S. 2008, ApJ, 687, 566
Malo, L., Artigau, É., Doyon, R., et al. 2014, ApJ, 788, 81
Mamajek, E. E. 2016, in IAU Symposium, Vol. 314, Young Stars & Planets Near the Sun, ed. J. H. Kastner, B. Stelzer, & S. A. Metchev, 21–26
Mamajek, E. E., Bartlett, J. L., Seifahrt, A., et al. 2013, AJ, 146, 154
Marcy, G. W., & Benitz, K. J. 1989, ApJ, 344, 441
Martin, C., & Mignard, F. 1998, A&A, 330, 585
Martín, E. L., Koresko, C. D., Kulkarni, S. R., Lane, B. F., & Wizinowich, P. L. 2000, ApJL, 529, L37
Martinache, F., Lloyd, J. P., Ireland, M. J., Yamada, R. S., & Tuthill, P. G. 2007, ApJ, 661, 496
Martinache, F., Rojas-Ayala, B., Ireland, M. J., Lloyd, J. P., & Tuthill, P. G. 2009, ApJ, 695, 1183
Mason, B. D., Hartkopf, W. I., Gies, D. R., Henry, T. J., & Helsel, J. W. 2009, AJ, 137, 3358
Mason, B. D., Hartkopf, W. I., Miles, K. N., et al. 2018, ArXiv e-prints, arXiv:1804.07845
Mazeh, T., Latham, D. W., Goldberg, E., et al. 2001, MNRAS, 325, 343
McAlister, H. A., Hartkopf, W. I., Hutter, D. J., & Franz, O. G. 1987, AJ, 93, 688
McCarthy, Jr., D. W. 1986, in Astrophysics of Brown Dwarfs, ed. M. C. Kafatos, R. S. Harrington, & S. P. Maran, 9–19
McLean, I. S., McGovern, M. R., Burgasser, A. J., et al. 2003, ApJ, 596, 561
Meyer, R. D., Horch, E. P., Ninkov, Z., van Altena, W. F., & Rothkopf, C. A. 2006, PASP, 118, 162
Monet, D. G., Levine, S. E., Canzian, B., et al. 2003, AJ, 125, 984
Montagnier, G., Ségransan, D., Beuzit, J.-L., et al. 2006, A&A, 460, L19
Montet, B. T., Crepp, J. R., Johnson, J. A., Howard, A. W., & Marcy, G. W. 2014, ApJ, 781, 28
Morgan, D. H. 1995, in Astronomical Society of the Pacific Conference Series, Vol. 84, IAU Colloq. 148: The Future Utilisation of Schmidt Telescopes, ed. J. Chapman, R. Cannon, S. Harrison, & B. Hidayat, 137
Nidever, D. L., Marcy, G. W., Butler, R. P., Fischer, D. A., & Vogt, S. S. 2002, ApJS, 141, 503
Patterson, R. J., Ianna, P. A., & Begam, M. C. 1998, AJ, 115, 1648
Perryman, M. A. C., Lindegren, L., Kovalevsky, J., et al. 1997, A&A, 323, L49
Platais, I., Pourbaix, D., Jorissen, A., et al. 2003, A&A, 397, 997
Pokorny, R. S., Jones, H. R. A., Hambly, N. C., & Pinfield, D. J. 2004, A&A, 421, 763
Pourbaix, D., Platais, I., Detournay, S., et al. 2003, A&A, 399, 1167
Pourbaix, D., Tokovinin, A. A., Batten, A. H., et al. 2004, A&A, 424, 727
Poveda, A., Herrera, M. A., Allen, C., Cordero, G., & Lavalley, C. 1994, RMxAA, 28, 43
Pravdo, S. H., & Shaklan, S. B. 2009, ApJ, 700, 623
Pravdo, S. H., Shaklan, S. B., Henry, T., & Benedict, G. F. 2004, ApJ, 617, 1323
Pravdo, S. H., Shaklan, S. B., Wiktorowicz, S. J., et al. 2006, ApJ, 649, 389
Raghavan, D., McAlister, H. A., Henry, T. J., et al. 2010, ApJS, 190, 1
Reid, I. N., Gizis, J. E., Kirkpatrick, J. D., & Koerner, D. W. 2001, AJ, 121, 489
Reid, I. N., Hawley, S. L., & Gizis, J. E. 1995, AJ, 110, 1838
Reid, I. N., Kilkenny, D., & Cruz, K. L. 2002, AJ, 123, 2822
Reid, I. N., Cruz, K. L., Laurie, S. P., et al. 2003, AJ, 125, 354
Reid, I. N., Cruz, K. L., Allen, P., et al. 2004, AJ, 128, 463
Reiners, A., & Basri, G. 2010, ApJ, 710, 924
Reiners, A., Joshi, N., & Goldman, B. 2012, AJ, 143, 93
Riddle, R. K., Priser, J. B., & Strand, K. A. 1971, Publications of the U.S. Naval Observatory Second Series, 20, 1
Riedel, A. R., Blunt, S. C., Lambrides, E. L., et al. 2017, AJ, 153, 95
Riedel, A. R., Murphy, S. J., Henry, T. J., et al. 2011, AJ, 142, 104

Riedel, A. R., Silverstein, M. L., Henry, T. J., et al. 2018, ArXiv e-prints, arXiv:1804.08812
Riedel, A. R., Subasavage, J. P., Finch, C. T., et al. 2010, AJ, 140, 897
Riedel, A. R., Finch, C. T., Henry, T. J., et al. 2014, AJ, 147, 85
Salim, S., & Gould, A. 2003, ApJ, 582, 1011
Schilbach, E., Röser, S., & Scholz, R.-D. 2009, A&A, 493, L27
Schmidt, S. J., Cruz, K. L., Bongiorno, B. J., Liebert, J., & Reid, I. N. 2007, AJ, 133, 2258
Schneider, A., Melis, C., Song, I., & Zuckerman, B. 2011, ApJ, 743, 109
Scholz, R.-D. 2010, A&A, 515, A92
Ségransan, D., Delfosse, X., Forveille, T., et al. 2000, A&A, 364, 665
Shakht, N. A. 1997, Astronomical and Astrophysical Transactions, 13, 327
Shkolnik, E. L., Anglada-Escudé, G., Liu, M. C., et al. 2012, ApJ, 758, 56
Shkolnik, E. L., Hebb, L., Liu, M. C., Reid, I. N., & Collier Cameron, A. 2010, ApJ, 716, 1522
Siegler, N., Close, L. M., Cruz, K. L., Martín, E. L., & Reid, I. N. 2005, ApJ, 621, 1023
Simons, D. A., Henry, T. J., & Kirkpatrick, J. D. 1996, AJ, 112, 2238
Skrutskie, M. F., Forrest, W. J., & Shure, M. 1989, AJ, 98, 1409
Skrutskie, M. F., Cutri, R. M., Stiening, R., et al. 2006, AJ, 131, 1163
Smart, R. L., Ioannidis, G., Jones, H. R. A., Bucciarelli, B., & Lattanzi, M. G. 2010, A&A, 514, A84
Smart, R. L., Lattanzi, M. G., Jahreiß, H., Bucciarelli, B., & Massone, G. 2007, A&A, 464, 787
Snodgrass, C., & Carry, B. 2013, The Messenger, 152, 14
Söderhjelm, S. 1999, A&A, 341, 121
Subasavage, J. P., Henry, T. J., Hambly, N. C., Brown, M. A., & Jao, W.-C. 2005a, AJ, 129, 413
Subasavage, J. P., Henry, T. J., Hambly, N. C., et al. 2005b, AJ, 130, 1658
Subasavage, J. P., Jao, W.-C., Henry, T. J., et al. 2009, AJ, 137, 4547
Subasavage, Jr., J. P. 2007, PhD thesis, Georgia State University
Tanner, A. M., Gelino, C. R., & Law, N. M. 2010, PASP, 122, 1195
Teegarden, B. J., Pravdo, S. H., Hicks, M., et al. 2003, ApJL, 589, L51
Teixeira, R., Ducourant, C., Chauvin, G., et al. 2009, A&A, 503, 281
Tinney, C. G. 1996, MNRAS, 281, 644
Tinney, C. G., Reid, I. N., Gizis, J., & Mould, J. R. 1995, AJ, 110, 3014
Tokovinin, A., & Lépine, S. 2012, AJ, 144, 102
Tokovinin, A., Mason, B. D., & Hartkopf, W. I. 2010, AJ, 139, 743
Tokovinin, A. A. 1992, A&A, 256, 121
van Altena, W. F., Lee, J. T., & Hoffleit, D. 1995, VizieR Online Data Catalog, 1174, 0
van Biesbroeck, G. 1974, ApJS, 28, 413
van de Kamp, P., & Worth, M. D. 1972, AJ, 77, 762
van Dessel, E., & Sinachopoulos, D. 1993, A&AS, 100, 517
van Leeuwen, F. 2007, A&A, 474, 653
von Braun, K., Boyajian, T. S., Kane, S. R., et al. 2011, ApJL, 729, L26
Wahhaj, Z., Liu, M. C., Biller, B. A., et al. 2011, ApJ, 729, 139
Wang, J., Fischer, D. A., Xie, J.-W., & Ciardi, D. R. 2014, ApJ, 791, 111
Ward-Duong, K., Patience, J., De Rosa, R. J., et al. 2015, MNRAS, 449, 2618
Weis, E. W. 1984, ApJS, 55, 289
—. 1986, AJ, 91, 626
—. 1987, AJ, 93, 451
—. 1988, Ap&SS, 142, 223
—. 1991a, AJ, 102, 1795
—. 1991b, AJ, 101, 1882
—. 1993, AJ, 105, 1962
—. 1994, AJ, 107, 1135
—. 1996, AJ, 112, 2300
—. 1999, AJ, 117, 3021
Weis, E. W., & Upgren, A. R. 1982, PASP, 94, 821
Winn, J. N., & Fabrycky, D. C. 2015, ARA&A, 53, 409
Winters, J. G., Henry, T. J., Jao, W.-C., et al. 2011, AJ, 141, 21
Winters, J. G., Henry, T. J., Lurie, J. C., et al. 2015, AJ, 149, 5
Winters, J. G., Sevrinsky, R. A., Jao, W.-C., et al. 2017, AJ, 153, 14
Winters, J. G., Irwin, J., Newton, E. R., et al. 2018, AJ, 155, 125
Woitas, J., Tamazian, V. S., Docobo, J. A., & Leinert, C. 2003, A&A, 406, 293
Worley, C. E. 1961, PASP, 73, 167
—. 1962, AJ, 67, 396
Young, A., Sadjadi, S., & Harlan, E. 1987, ApJ, 314, 272
Zechmeister, M., Kürster, M., & Endl, M. 2009, A&A, 505, 859